THE PENNSYLVANIA STATE UNIVERSITY
SCHREYER HONORS COLLEGE

DIVISION OF ENGINEERING, BUSINESS, AND COMPUTING

Multiphysics Finite Element Analysis of Lightning Strike Effects on Carbon Fiber Reinforced Polymer Composites

CHRISTOPHER TRAPP
SPRING 2021

A thesis
submitted in partial fulfillment
of the requirements
for a baccalaureate degree
in Mechanical Engineering
with honors in Mechanical Engineering

Reviewed and approved* by the following:

Amir Barakati
Associate Teaching Professor of Mechanical Engineering
Thesis Supervisor

Joseph M. Mahoney
Associate Professor of Mechanical Engineering and Kinesiology
Thesis Co-supervisor

Sandy Feinstein
Professor of English
Honors Advisor

* Electronic approvals are on file.

Abstract

Use of advanced composite materials in aircraft has increased in recent years. The materials have high specific strength that allows for aircraft designs to be made more fuel efficient. A drawback of carbon fiber reinforced polymer (CFRP) composites compared to traditional aircraft materials like aluminum is increased susceptibility to damage under lightning strike. Damage effects of lightning strike on composites can include resin decomposition, fiber breakage, and delamination. To better understand the phenomenon and address the concern of lightning strike damage, researchers have performed experimental and numerical lightning strike simulations on composite materials with and without protection methods. Finite element analysis has been found to be a helpful tool in modeling and analyzing the lightning strike event. Here, a model was successfully developed replicating a published work to simulate the damage effects of lightning current components C and D on a CFRP composite laminate with a fastener. The results of the replication model were validated through comparison with the published results. The model was then modified to make decomposition damage predictions with the presence of a copper outer layer and, separately, with different stacking sequences. It was found that increasing the thickness of the copper layer led to decreased temperatures in the CFRP laminate. Damage on the top surface of the laminate was found to develop differently under different current components. It was also found that adjacent layers with similar or matching fiber orientations can lead to longer decomposition damage under current component D.

Table of Contents

List of Figures

List of Tables

Acknowledgments

I thank Dr. Amir Barakati for the time he devoted to meet with me virtually on a weekly basis, even during the summer months, to discuss the progress of this thesis and the computational simulations involved. I thank Dr. Joseph M. Mahoney for the helpful information he gave me about thesis formatting and using LaTeX. I thank all in my thesis committee, Dr. Amir Barakati, Dr. Joseph M. Mahoney, and Dr. Sandy Feinstein, for their help in reviewing this thesis. Lastly, I thank my parents for their support of my education.

Computations for this research were performed on the Pennsylvania State University's Institute for Computational and Data Sciences' Roar supercomputer.

Chapter 1

Introduction

Advanced materials are a key focus in the field of engineering today. In the progression towards more efficient and sustainable designs, materials called *composites*, which are materials that consist of two or more constituents, are being developed and employed because of their superior material properties to those of traditional materials [1]. Composites are seeing use in a variety of different fields with a significant one being the aerospace industry [2]. However, with the improvements that composite materials bring, they may also have significant drawbacks that must be addressed. Damage analysis of composites can be a complicated process given their advanced nature. In the case of composite panels used in aircraft structures, the question arises of how well the composite will hold up under a lightning strike. This chapter provides a brief overview of composites and the lightning strike phenomenon and a review of the literature examining the effects of lightning strikes on composite materials.

The most general definition of a composite material is any material that is made up of two or more constituents [1]. However, a more refined definition may be used to narrow the possibilities of what may be considered a composite and what may not. Chawla identifies three criteria for a composite material: (1) it must be manufactured, (2) involve two or more distinct constituents, and (3) feature unique properties separate from those of the constituents by themselves [3]. Composite materials generally consist of a reinforcement material and a matrix material. The reinforcement material is usually strong but brittle. The matrix material is continuous and acts to hold the composite together [1]. In the case of a carbon fiber reinforced polymer (CFRP) composite, the carbon fibers are the reinforcement material while the polymer resin is the matrix material.

In aircraft, composite materials are replacing conventional materials like steel because of their superior material properties [1]. Composite materials can be designed to have a higher specific strength compared to steel, which is the strength to weight ratio. Reducing the weight of the aircraft promotes greater fuel efficiency and maneuverability. Composites are also used by the aerospace industry because they can be corrosion and fatigue resistant [4]. Composite materials contribute to over 50% of the overall mass of the Boeing 787 and the Airbus A350 [5]. The composites used in modern aircraft are polymer matrix composites [6], meaning the matrix is made of a polymer like epoxy. In addition to aerospace applications, composites are seeing increased use in civil engineering, automotive, medical, and sports applications [1]. They are also used in wind turbine blades [4].

In addition to their potentially superior material properties, composites can also add an element of flexibility to the engineering design process. Using conventional materials sometimes leaves little room for variation in design because of constraints posed by the material's properties. With the introduction of composites, more design options may become available. While conventional materials may offer only a limited selection of choices and treatments, the composite material provides more ways in which it can be tailored to meet the demands of the specific design [3]. However, with more variables, more attention to detail is necessary. For example, the orientation of the fibers in a fiber reinforced composite will determine the direction in which the material has the most strength [4].

Since the design of the composite material can vary with the design of the product it is a part of, all properties of the composite should be considered. Carbon fibers alone are good electrical conductors. However, the polymer matrix may not share this same conductivity. Therefore, the CFRP composite may be a good electrical conductor in the direction of the fibers, but a poor electrical conductor in the direction perpendicular to the fiber plane. The material has a lower overall electrical conductivity than the metals used in the past in aircraft like aluminum [2, 7]. Lower conductivity can lead to decreased protection against lightning strikes.

Commercial aircraft are struck by lightning on average about once every year [6, 8]. In-flight studies using test aircraft have been performed that collected data on lightning strike events [9]. A particular test aircraft used by NASA, an F-106B, encountered 714 lightning strikes between 1980 and 1986 [9]. During a single lightning strike on an aircraft in flight, the lightning may switch between multiple, discrete attachment points in a sweeping motion from the front to the rear of the aircraft. As a result, the total energy of the lightning flash is distributed over the multiple attachment points [10]. Attachment points are locations where the lightning current either enters or exits the aircraft, and these tend to be the outermost points of the aircraft [11]. Some locations on the aircraft are more likely to experience a lightning strike attachment than others. Consequently, different lightning strike zones have been defined [12] as well as different lightning current components [10].

The lightning strike zones for commercial aircraft have been outlined in the SAE ARP5414B standard [12]. In addition to the lightning strike zones, four different lightning current components have been defined: current components A, B, C, and D, corresponding to first return stroke, intermediate current, continuing current, and subsequent return stroke, respectively. These are explained in the SAE ARP5412B standard and are depicted in Fig. 1.1. A return stroke is a distinct pulse of current encountered in a lightning flash. Therefore, current components A and D are characterized by a high peak current and low duration. In some lightning flashes, a return stroke may be followed by an intermediate current and then possibly a continuing current, which are depicted by current components B and C, respectively [10]. While Fig. 1.1 shows a general organization of the different current components, it should be recognized that lightning flashes are not restricted to four distinct current components and may contain several subsequent strokes and following intermediate and continuing currents. Current components have often been simulated in

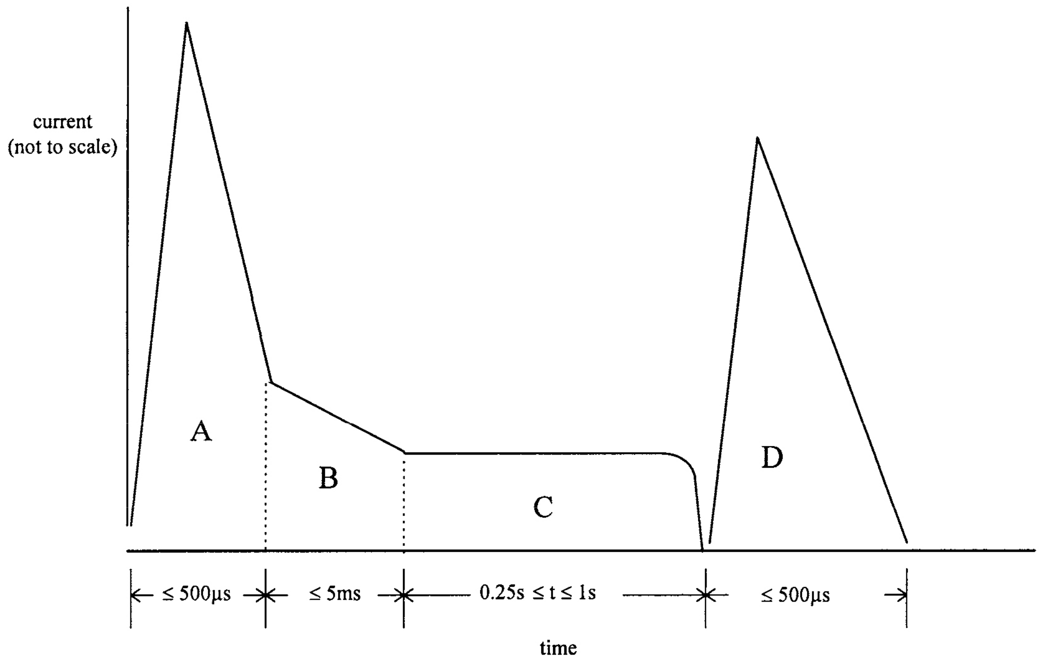

Figure 1.1: Lightning current components from SAE ARP5412B [10].

isolation, but they have also been simulated together (*i.e.* sequentially) [13–15].

If an aircraft has an exterior that is a good conductor of electricity, the lightning current will be more likely to remain on the exterior and cause little damage [6]. An example of an exterior that is a good electrical conductor is an aluminum skin [2]. If the outer surface is made of a less electrically conductive material, a lightning strike is more likely to cause significant damage. The lightning current will seek the path of least resistance and may travel through the aircraft structure. The lightning current may vaporize control cables, weld hinges, and ignite fuel vapors inside fuel tanks, which are considered direct effects [2, 6, 9]. Fuel vapor ignition is especially a concern when the fuel cell is made of a composite material because this increases the risk of a spark due to the lightning strike [8]. Indirect effects include interference and disablement of electronic equipment [9]. Aircraft designers have come up with ways to protect interior components and occupants from these dangers [16].

The general premise of lightning strike protection (LSP) is to keep the lightning current on the exterior of the aircraft so that it passes by without significant damage. This helps protect against both direct and indirect effects. Designing for adequate LSP involves using materials that have high conductivity [2, 8]. A traditional method of protecting composites from lightning strike involves adding a metal structure in the form of either strips or a mesh. The metal structure has a high conductivity and helps to limit the amount of lightning strike damage [2]. Metals used are aluminum and copper because of their low cost compared to other metals with high specific electrical conductivity [8]. The downside of applying a metal structure is that it increases weight, which acts against the weight savings that composite materials provide. Manufacturing the protective structures also increases cost. Other novel approaches to solving the problem of lightning protection have been introduced. These approaches include using carbon nanotubes and increasing the conductivity of the epoxy used in the CFRP [2]. Some of these new approaches have been the subject of recent research, which will now be discussed.

To date, numerous studies have been conducted to elucidate the nature and damage effects of lightning strikes on composite materials and to test LSP methods [6, 7, 13–15, 17–71]. These studies have involved experimental testing, computational and/or mathematical analyses, or a combination of both. Feraboli et al. presented experimental studies on the damage effects on carbon fiber/epoxy composites of simulated lightning current modeled after lightning current component D. The tests compared effects with and without a fastener at the point of lightning strike attachment and with a comparable mechanical impact [7, 17]. Hirano et al. presented an experimental study on the damage effects on graphite/epoxy composites by simulated lightning current component A. They identified the three damage modes of (1) fiber damage, (2) resin deterioration, and (3) internal delamination [18]. Ogasawara et al. published a finite element thermal-electrical coupled model based on the experiments of Hirano et al. that showed agreement with the delamination damage area. The model features changing electrical conductivity in the thickness direction of the laminate with change in temperature. The model also incorporates a virtual latent heat at 3000°C to simulate fiber breakage due to sublimation [19]. Many subsequent numerical studies have used a coupled thermal-electrical model.

Chemartin et al. published a study in 2012 that analyzed the lightning arc and the corresponding damage effects on aircraft panels experimentally and numerically. They analyzed thermal and mechanical damage effects of aluminum and composite panels with and without a paint layer. They also examined current distribution when simulated lightning attaches to an aircraft fastener [20]. Abdelal and Murphy published a coupled thermal-electrical analysis of thermal damage that considered nonlinear temperature-dependent material properties. They included a comparison of the resulting damage effects with and without a copper mesh for LSP [21]. Munoz et al. performed an experimental and computational study that built upon the coupled thermal-electrical model to also examine mechanical damage effects caused by magnetic and acoustic pressures. It did not include coupling between the thermal-electrical physics and the mechanical physics [22]. Wang F. S. et al. published a thermal-electrical-mechanical model involving deletion of ablated elements. The model was used to estimate difference in residual strength before and after the lightning strike [23].

Modeling of the lightning strike event continued to be explored and become more advanced. Liu et al. published an experimental and numerical study including a finite element analysis that combined both a thermal-electrical analysis and a blow-off impulse (BOI) analysis. The BOI effect is caused by pyrolysis of the resin and decomposition of fibers as a result of extremely high temperature and was not considered in previous papers [24]. Dong et al. published a study featuring a coupled electrical-thermal-pyrolytic finite element model, which built on the coupled thermal-electric model by also considering change in material properties based on resin pyrolysis degree [25]. Dong et al. continued use of the thermal-electrical-pyrolysis model to explore the effects of varying the electrical and thermal conductivities of the CFRP composite, and they concluded that increasing the electrical conductivity has a significant effect on reducing the predicted damage volume [26]. At a similar time, Han et al. developed a carbon nanotube buckypaper added as a conductive layer for LSP and studied its behavior experimentally and with finite element analysis [27], Li et al. experimentally examined the effects of simulated lightning strike on a woven fabric CFRP composite [28], and Ma et al. proposed analytical models for designing a CFRP composite with carbon nanotubes for lightning strike resistance [29]. Later, Hirano et al. developed and experimentally evaluated a conducting thermosetting resin in a CFRP composite for LSP [30].

Wang Y. and Zhupanska presented a thermal-electric finite element model with element deletion involving non-uniform applied current density and applied heat flux that varied both spatially and temporally [31]. Soykasap et al. used coupled thermal-electrical finite element analysis to compare damage effects with and without carbon nanotube doping [32]. Wang F. S. et al. published a study in which a thermal-electrical-mechanical analysis with element deletion was used to examine ablation damage in four types of CFRP composites: without protection and with three different aluminum coating protection types [33]. Naghipour et al. examined delamination damage in CFRP composites in a finite element study using interlaminar elements of zero thickness [34]. Shulin et al. used a thermal-electrical model with temperature-dependent material properties caused by resin pyrolysis and evaluated damage penetration time by laminate layer [35]. Yin et al. used a thermal-electrical model to examine lightning strike damage effects, including temperature and electric potential distribution, about a fastener in a CFRP composite [36].

Research has continued in recent years to further develop the lightning strike model and explore different LSP methods. In 2017, Fu et al. compared LSP methods using a thermal-electrical model considering dielectric breakdown of the LSP [37]. Dong et al. continued the use of a thermal-electrical-pyrolytic model to explore lightning damage in CFRP composites with interlayers containing nickel-coated multi-walled carbon nanotubes (Ni-MWCNTs). The study found that increasing the number of Ni-MWCNT interlayers with higher electrical conductivity led to improved LSP [38]. Yin et al. published an experimental and numerical study using a thermal-electrical model to predict ablation damage in carbon woven fabric/epoxy laminates rather than in CFRP composites with unidirectional fibers [39]. Guo et al. published a finite element study comparing temperature field and pyrolysis field methods and concluded that the temperature-dependent model is suitable for predicting in-plane damage while the pyrolysis dependent model is suitable for predicting in-depth damage [40]. Abdelal and Murphy developed a model of the thermal plasma during a simulated lightning strike event [41]. During the same year, Katunin et al. developed and tested experimentally a CFRP composite with an electrically conductive PANI/epoxy matrix for LSP [42–44].

In 2018, Wang F. S. et al. used finite element analysis to compare residual strength damage of CFRP composites by lightning strike [45]. Wang B. et al. published a study of a LSP method consisting of an enriched graphene surface for CFRP composites and used finite element analysis, in addition to experimental tests, to analyze the benefits of the LSP [46]. Kirchdoerfer et al. used finite element analysis to examine the shock physics in an aircraft fastener assembly when struck by lightning [47]. Kamiyama et al. used a finite element model involving thermal decomposition and considering the cooling process to examine delamination damage in CFRP composites exposed to lightning strike [48]. Che et al. examined experimentally the LSP effectiveness of CFRP composites with cold sprayed metallic coatings [49]. Chen H. et al. published a study using finite volume analysis with magneto hydro dynamics equations to model the lightning channel and finite element analysis to solve for the resulting temperature distribution in the CFRP composite [50]. Lee et al. used finite element analysis to compare thermal damage on a carbon/epoxy composite unprotected, with a copper mesh, and with a pitch carbon fiber paper (PCFP) [51]. Shortly after, Lee et al. published an additional study comparing thermal damage based on models of past literature [52]. Dong et al. published a finite element study analyzing thermal ablation and expansion from lightning strike using thermal-electrical coupling, pyrolysis equations, and thermal-mechanical coupling [53]. Foster et al. published two works in which they used finite element analysis to model lightning arc attachment and mechanical effects caused by thermal expansion, respectively [54, 55]. The following year, Foster et al. published an additional work modeling the mechanical effects caused by pressure loading [56].

The year 2019 saw further development of aspects of the lightning model that had been introduced in previous years. Jia et al. published a study furthering examination of the BOI effect involving a finite element model with both thermal-electrical and BOI analyses. They identified changes caused by the BOI effect in Joule heating damage distribution, multiple damage forms presented by the BOI effect, and an isotropic mechanical behavior of the composite at high pressure [57]. Lee et al. published a study examining the effect of changing parameters of a PCFP protection layer had on reducing lightning strike damage and found that a higher in-plane conductivity decreased damage [58]. Later, Lee et al. published a study predicting mechanical damage in CFRP composites due to lightning strike using shock wave overpressure and air blast overpressure [59]. Fu and Ye published a numerical study involving a plasma expansion model to examine mechanical damage in a CFRP composite with LSP struck by lightning [60]. Zhang et al. used experimentation and a thermal-electrical finite element analysis to examine the protection offered by carbon nanotube films experimentally and numerically with thermal-electrical finite element analysis [61]. Dong et al. published a finite element study involving an applied electric current with a Gaussian distribution and heat flux for analysis of carbon fiber composites exposed to simulated lightning strike current component D or both current components D and C [14]. Hu and Yu simulated lightning strike on a CFRP composite with a copper mesh as LSP experimentally and numerically [71], and Wang F. S. et al. used finite element analysis to study the effectiveness of copper mesh and aluminum mesh as LSP [62]. Millen et al. published a study involving a preceding plasma model used to determine boundary conditions for a thermal-electrical model [63]. Millen et al. then furthered this work to develop a progressive damage model involving a preceding plasma model, a thermal-electrical model, and a temperature-displacement model to examine thermal and mechanical damage [64].

In 2020, Millen et al. estimated thermal damage on composite specimens using a preceding plasma model and subsequent thermal-electrical model while considering the effect had on the plasma by specimen properties [65]. Millen and Murphy also published a study analyzing cases of different boundary conditions from literature using two simulation techniques to examine thermal and mechanical damage [66]. Sun et al. validated a thermal-electrical-structural finite element analysis with dynamic conductivities of the CFRP composite with comparison to experimental results [67]. More recently, Lee et al. published a finite element study examining lightning damage effects produced by electric current and mechanical forces due to electromagnetics and acoustics. The study also featured radial and asymmetric arc channel expansion [68].

In addition, Chen J. et al. published an experimental and numerical study of a composite laminate with a fastener exposed to simulated lightning strike components C and D. They proposed numerical modeling using thermal-electrical coupling that includes both electrical current and heat flux loads. They evaluated experimental damage through ultrasonic testing, identified regions of resin decomposition, and validated their numerical simulation through comparison with their experimental results [69].

The review of the literature shows that numerous experimental and numerical studies have been performed in recent years to examine lightning strike damage in CFRP composite laminates and evaluate different methods of LSP, such as the application of carbon nanotubes. A common theme among the numerical studies listed is the use of a *coupled* thermal-electrical or thermal-electrical-mechanical model to simulate the damage effects in a CFRP composite laminate [14, 19, 21–27, 31–33, 35–40, 45, 46, 48, 50–55, 57, 58, 61–71]. While the models used in these studies vary in complexity and scope, they all consider the Joule heating phenomenon, which involves multiple physical fields. Therefore, a multiphysics approach is commonly deemed necessary for effective modeling. Many of the numerical simulations were performed using commercial finite element analysis software such as Abaqus, Ansys, or COMSOL. These software packages allow for complex finite element analysis models to be set up and run with relative ease compared to writing code to perform the same analysis. Many of the studies that used these software packages provide adequate information in their publications to allow for replication.

Only a limited number of studies have analyzed the damage effects of simulated lightning strike on a CFRP composite laminate with a fastener [7, 17, 20, 33, 36, 44, 47, 69]. None of these studies specifically involved adding a solid copper outer layer or using different laminate stacking sequences to examine changes in decomposition damage. Given their high conductivity, metallic fasteners present a likely point of lightning strike attachment in composite aircraft panels [36, 47]. Because of the common use of metallic fasteners in aircraft structures [36, 47], it is appropriate to examine the damage caused by a simulated lightning strike on a fastener in a CFRP composite laminate in addition to the damage in unnotched composite laminates. Furthermore, the development of a finite element model of the simulated lightning strike event allows for damage predictions to be made with less equipment and cost and in less time compared to experimental testing.

This thesis seeks to first replicate the recent numerical finite element analysis simulations performed by Chen J. et al., which predict the decomposition damage effects in a CFRP composite laminate with fastener subjected to lightning strike current components C and D. The analyses involve the coupling of thermal and electrical physics. The numerical simulation results are compared to the published results of the original study. Following model validation, extensions of the study are performed to explore novel configurations of the model and numerically predict changes in lightning strike damage in the CFRP composite laminate. These extensions include applying a copper outer layer and, separately, using different laminate stacking sequences. Chapter 2 presents background information about carbon fiber reinforced polymer composites and finite element analysis. Chapter 3 details the methods used to perform the numerical simulations in this thesis. The results of the simulations are presented in Chapter 4 and discussed in Chapter 5. Finally, Chapter 6 presents the conclusions of the work herein and potential future research directions.

Chapter 2

Background

This chapter presents further information on carbon fiber reinforced composites and finite element analysis. The material properties of carbon fiber reinforced composites are discussed. Then, the general procedure of finite element analysis is given. The background information provided in this chapter is important for understanding the methods used to perform the numerical simulations of this thesis.

2.1 Carbon Fiber Reinforced Polymer Composites

As introduced in Chapter 1, composites have material properties that can be anisotropic (*e.g.*, electrical conductivity). In fiber-reinforced composites, the greatest strength of the composite is in the direction of the fibers. Because the strength depends on direction, designs may implement layering to maximize the effectiveness of the fiber-reinforced composite for its intended purpose. An individual layer is called a "lamina," or a "ply," while the complete stack is called a "laminate." If strength is needed in more than one direction, the laminae may be stacked so that the fibers run at different angles with respect to one another. The order of stacking is referred to as the "stacking sequence" [72].

Understanding stacking sequence notation is important for communicating the layup of a composite laminate. Stacking sequence notation expresses the angle at which the fibers of each lamina are oriented with respect to one another. It also takes note of any repetition and symmetry that may be present to shorten notation, if possible. Suppose a laminate has the stacking sequence $[45°/0°/-45°/90°]$, which is visualized in Fig. 2.1. Such a laminate consists of four laminae. The fibers of the top lamina are rotated 45° from a zero axis (following the axes shown in Fig. 2.1, the x-axis is the zero axis) in the plane normal to the laminate thickness. The next lamina below has no rotation, meaning the fibers are aligned with the zero axis. The next two laminae have fibers rotated at angles of -45° and 90°, respectively, to the zero axis [72]. Laminates with this

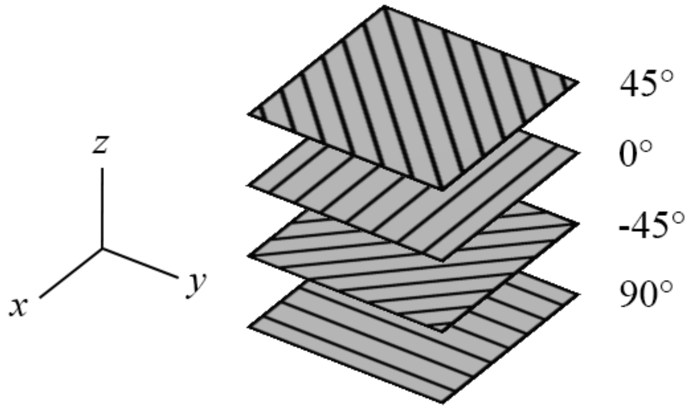

Figure 2.1: Diagram of composite laminate with stacking sequence of $[45°/0°/-45°/90°]$. The lines show the direction of the fibers in each layer.

stacking sequence may be called quasi-isotropic because multiple fiber orientations are used to make the laminate stronger in multiple directions [5]. If the sequence is mirrored to include four more laminae, the laminate exhibits symmetry and may be given the notation of $[45°/0°/-45°/90°]_S$. If the sequence is repeated once before the line of symmetry, the subscript would include a "2" before the "S." More details can be expressed through this notation, such as lamina thickness, if necessary [72].

To analyze a complete composite laminate, the fibers and polymer of each lamina are generally modeled as a single, homogeneous solid with orthotropic material properties [3]. An orthotropic material has material properties that are unique along the three perpendicular coordinate axes. In a unidirectional fiber-reinforced composite lamina, the fiber axis is x_1, the axis perpendicular to the fibers in the lamina plane is x_2, and the axis perpendicular to the lamina plane is x_3 [73]. These axes are depicted in Fig. 2.2, in which the circles represent the cross sections of the fibers.

Because orthotropic materials have different material properties depending on direction, they

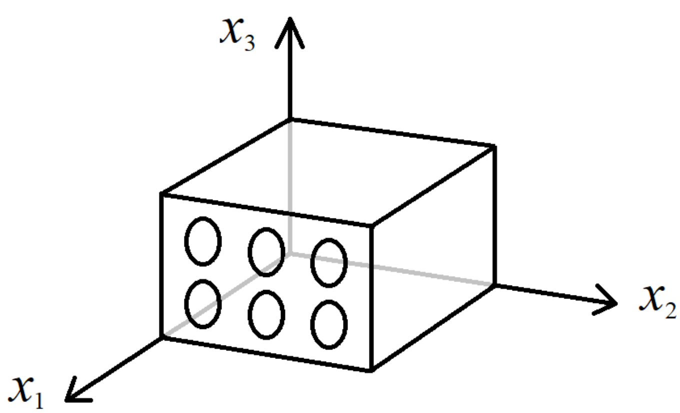

Figure 2.2: Diagram of unidirectional fiber reinforced composite lamina.

have more independent material properties compared to isotropic materials. In an isotropic material, material properties are designated with a single value as direction has no influence. An example is Young's modulus, E. In orthotropic materials, material properties are defined for each one of the three perpendicular directions of orthotropy. Assuming the material exhibits orthotropy in elasticity, Young's modulus is defined by three values: E_1, E_2, and E_3, respective to the directions of orthotropy. The orthotropic material properties may be presented in a 3-by-3 matrix. If the axes of orthotropy are aligned with those of the coordinate system, Young's modulus matrix, $\mathbf{E}$, may be represented as shown in Eq. (2.1).

$$\mathbf{E} = \begin{bmatrix} E_{11} & 0 & 0 \\ 0 & E_{22} & 0 \\ 0 & 0 & E_{33} \end{bmatrix} \tag{2.1}$$

Similarly, for other mechanical material properties, there are three unique values each for Poisson's ratio, ν, and for shear modulus, G. For orthotropic materials, there are nine independent elastic constants for structural mechanics [73]. The mechanical properties are related to one another through the stress-strain relationship described by Hooke's law in Eq. (2.2).

$$\boldsymbol{\sigma} = \mathbf{C}\boldsymbol{\epsilon} \tag{2.2}$$

In this equation, $\boldsymbol{\sigma}$ is stress, $\boldsymbol{\epsilon}$ is strain, and $\mathbf{C}$ is a stiffness matrix that relates the two. The equation expanded for an orthotropic material is shown in Eq. (2.3) in matrix form and with Voigt notation. The constants of the stiffness matrix, $\mathbf{C}$, are dependent on E, ν, and G in different material directions. The inverse of the stiffness matrix is referred to as the compliance matrix and is denoted by $\mathbf{S}$ [73].

$$\begin{bmatrix} \sigma_1 \\ \sigma_2 \\ \sigma_3 \\ \sigma_4 \\ \sigma_5 \\ \sigma_6 \end{bmatrix} = \begin{bmatrix} C_{11} & C_{12} & C_{13} & 0 & 0 & 0 \\ C_{21} & C_{22} & C_{23} & 0 & 0 & 0 \\ C_{31} & C_{32} & C_{33} & 0 & 0 & 0 \\ 0 & 0 & 0 & C_{44} & 0 & 0 \\ 0 & 0 & 0 & 0 & C_{55} & 0 \\ 0 & 0 & 0 & 0 & 0 & C_{66} \end{bmatrix} \begin{bmatrix} \epsilon_1 \\ \epsilon_2 \\ \epsilon_3 \\ \epsilon_4 \\ \epsilon_5 \\ \epsilon_6 \end{bmatrix} \tag{2.3}$$

While a material may be orthotropic in terms of its mechanical properties, it can also be orthotropic in terms of other material properties. For a carbon fiber reinforced polymer composite, these additional properties include thermal conductivity and electrical conductivity. As discussed in Chapter 1, carbon fibers are good electrical conductors while matrix resins are generally not [2]. The electrical conductivity of a unidirectional CFRP lamina, examined as a homogeneous solid, is good in the direction of the fibers and poor in the directions perpendicular to the fibers. In terms of three orthogonal axes, the electrical conductivity in the fiber direction, σ_1, is large, while σ_2 and σ_3 are small. It is possible to have a bidirectional lamina or woven lamina containing fibers running in two or more directions, respectively. In these cases, the distribution of electrical conductivity may be different. If aligned with the coordinate axes, the electrical conductivity matrix, $\boldsymbol{\sigma}$, is represented as shown in Eq. (2.4).

$$\boldsymbol{\sigma} = \begin{bmatrix} \sigma_{11} & 0 & 0 \\ 0 & \sigma_{22} & 0 \\ 0 & 0 & \sigma_{33} \end{bmatrix} \tag{2.4}$$

As mentioned, *thermal* conductivity is another material property that is orthotropic in CFRP laminae. The carbon fibers and the matrix material generally exhibit a difference in thermal conductivity. As with electrical conductivity, the thermal conductivity is greater in the direction of the fibers. If aligned with the coordinate axes, the thermal conductivity matrix, $\mathbf{k}$, is represented by Eq. (2.5).

$$\mathbf{k} = \begin{bmatrix} k_{11} & 0 & 0 \\ 0 & k_{22} & 0 \\ 0 & 0 & k_{33} \end{bmatrix} \tag{2.5}$$

For the matrices $\boldsymbol{\sigma}$ and $\mathbf{k}$ listed here, it is assumed that the orthotropic axes of the material properties are aligned with the coordinate axes. While this can greatly simplify defining the material properties and performing calculations, it does not have to be the case. A composite laminate may consist of multiple plies that each have fibers oriented in different directions, such as the example provided earlier in this section. To define the material properties of the plies with different orientations, it may be necessary to use coordinate transformations.

It can be seen that modeling CFRP composites can be a complicated task. Needing to consider the fiber direction and the orthotropy that accompanies it, problems involving CFRP composites can be more complex than those involving only isotropic materials. Fortunately, finite element analysis is an available tool that can be helpful for solving problems with CFRP composites.

2.2 Finite Element Analysis

Often in engineering, there are problems that cannot be solved using an analytical problem-solving method that yields an exact solution. Many real-world problems are too complex and include too many variables to be modeled simply enough for an analytical solution. For complex problems that demand precise answers, it may be necessary to use a numerical approach so that more contributing factors can be considered in the model with the solving resources that are available. The process of numerical simulation generally involves transforming a governing system of differential equations into algebraic expressions that are then solved computationally [74]. The solution may not be exact, but it may be closer to reality than if assumptions are made to obtain an exact solution.

Finite element analysis is a numerical technique that involves breaking a domain into subdomains and solving a system of equations that relate and link the subdomains. These subdomains are called “finite elements.” In addition to elements, certain points, called “nodes,” are defined in each element [74]. The discretized model of elements and nodes is called a “mesh” [75]. The process of breaking the model into elements is called discretization because it involves turning a continuous model into a discrete one. Finite element analysis involves performing approximations over a discrete number of elements to produce an approximate solution for the problem being solved. In this section, a brief history and the general process of the finite element method, including the process of mesh convergence, will be discussed. In addition, the physics equations used in the simulations herein will be presented.

Finite element analysis was born out of aerospace research for engineering wing technology in the 1950s. Among the early contributors are Jon Turner and John Argyris. The first time the term finite element method was mentioned in a published paper was in the year 1960 by Ray

Clough. Performance of computationally-rigorous finite element simulations are common in research today with modern computer technology, but they were difficult with the technology available in the early stages of finite element research [75].

With the finite element method experiencing more attention as computer technology becomes more advanced, several authors have written about the process of the method in recent years [73–75]. In general, the process begins by first forming a model of the problem and then discretizing the model into finite elements. Modeling involves creating a representation of the physical subject that is to be simulated. Models can vary in number of dimensions and complexity depending on the requirements of the simulation. Boundary conditions, which explain what happens at the edges of the model domain [75], are defined during model formation. Models can be discretized into only a few elements, tens of thousands of elements, or even more. Increasing the number of elements increases the accuracy of the simulation up to a point, but it also increases the amount of computational power and time necessary to solve the model. The goal of effective discretization is to accurately represent the event that is being simulated without wasting computational resources. Some commercial finite element software feature discretization that produces a fine mesh at locations of interest and a coarse mesh elsewhere, which reserves computational resources for the parts of the simulation that are most critical.

With the mesh formed, the next step involves forming element equations based on the governing physics equations to solve a specific unknown. This unknown depends on the physics equations being used; for example, in a structural mechanics problem, the unknown may be displacement. Interpolation functions are used to approximate over the elements. Different interpolation functions, such as linear or quadratic, can be used. The element equations are then assembled into a global system to which boundary conditions can be applied and the unknown solved for [73]. Since the number of element equations and the size of the assembled global system is related to the number of elements, the system may be impossible or impractical to solve by hand. Therefore, it is commonly represented in matrix form, making it easier to be processed and solved by a computer.

It is possible to follow the general steps listed above and obtain a solution for a model. However, given the numerical nature of finite element analysis, it is important to confirm that a sufficient number of elements were used through a process called mesh convergence. In this procedure, the mesh is repeatedly refined and the solution recorded for each subsequent mesh. Once a sufficient number of elements is used, the results should exhibit differences between one another that are insignificant. The point at which the differences are negligible indicates the number of elements that should be used. A visual example of mesh refinement of a beam is shown in Fig. 2.3. A similar process, which involves refining the time step of the solver, can be followed for transient models.

As mentioned previously, governing physics equations are necessary to form and solve the system of equations used in finite element analysis. The simulations performed in this thesis involve electrical and thermal physics as well as thermal-electric coupling. The equations presented here are those used by the COMSOL Multiphysics software and described in its documentation [76, 77]. First, the electrical physics equations will be discussed. The principle of conservation of charge is used to determine the electric potential throughout the model at different instances in time. The principle states that the charge entering or leaving a volume is equal to the change in charge of that volume. The equation for the conservation of charge is shown in differential form in Eq. (2.6).

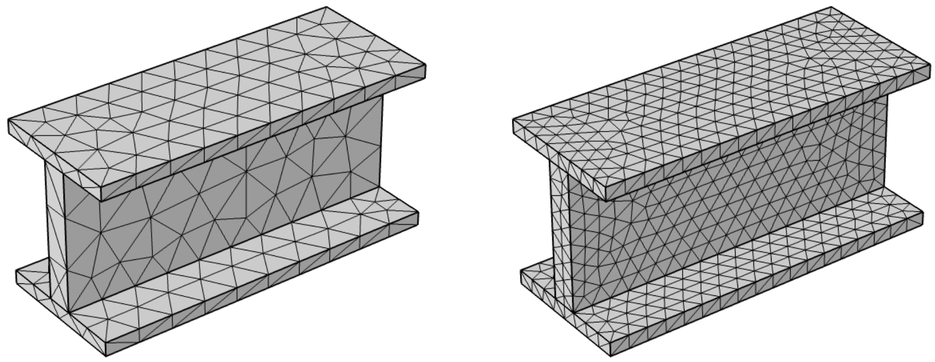

Figure 2.3: Example of mesh refinement from coarse (left) to fine (right).

$$\nabla \cdot \mathbf{J} = -\frac{\partial \rho}{\partial t} \tag{2.6}$$

Here, $\mathbf{J}$ represents current density, ρ represents charge density, and t is time. In similar differential form, Ohm's law is expressed by Eq. (2.7) for the transient case.

$$\mathbf{J} = \sigma \mathbf{E} + \frac{\partial \mathbf{D}}{\partial t} + \mathbf{J}_e \tag{2.7}$$

In this equation, σ is the electrical conductivity of the medium, $\mathbf{E}$ is electric field, $\mathbf{D}$ is electric displacement, and $\mathbf{J}_e$ is externally generated current density. Lastly, the electric potential, V, is defined by the relation in Eq. (2.8).

$$\mathbf{E} = -\nabla V \tag{2.8}$$

The simulations also account for heat transfer both spatially and temporally. The heat equation, shown in Eq. (2.9), is used in the finite element analysis process to determine the temperature, T, throughout the discretized domain.

$$\rho C_p \left(\frac{\partial T}{\partial t} + \mathbf{u} \cdot \nabla T \right) + \nabla \cdot \mathbf{q} = Q \tag{2.9}$$

In this equation, ρ represents density of the material, C_p is heat capacity at constant pressure, $\mathbf{u}$ is velocity field, $\mathbf{q}$ is heat flux, and Q is heat source. Heat flux is solved using Fourier's law of thermal conduction, which is shown in Eq. (2.10).

$$\mathbf{q} = -k \nabla T \tag{2.10}$$

Above, heat flux is related to the thermal conductivity, k, of the material and the temperature gradient, ∇T. The simulations also involve thermal-electric coupling in the form of Joule heating, as shown in Eq. (2.11).

$$Q_e = \mathbf{J} \cdot \mathbf{E} \tag{2.11}$$

The resistive heating, Q_e, is calculated using current density, $\mathbf{J}$, and electric field, $\mathbf{E}$. The resistive heating is then accounted for in the heat equation as a heat source.

The governing physics equations here make it possible to form and solve the system of equations for finite element analysis. The governing physics equations involve matrices and differentials, which add to the complexity of the problem being solved. This is one of the reasons it can be helpful or necessary to use finite element analysis with the aid of software to computationally simulate a lightning strike event. Chapter 3 will discuss the methods used to set up and perform the finite element simulations in COMSOL Multiphysics.

Chapter 3

Methods

In this chapter, the methods used to build and perform the numerical lightning strike simulations are explained. These simulations, performed using finite element analysis, include practice simulations, replication of the simulations of a published work, and extensions using the developed simulation model.

The finite element simulations detailed in this chapter were performed using COMSOL Multiphysics (Burlington, MA, v5.4) [76]. The software was accessed via a remote connection to the Roar supercomputer of the Pennsylvania State University[1]. The line plots in this Chapter and in Chapter 4 were produced with MATLAB (Natick, MA, R2020b) [78]. MATLAB was also used to perform calculations in developing a waveform equation for current component D.

3.1 Practice Simulations

Various practice simulations were performed to develop understanding of the COMSOL finite element analysis software. First, a problem that could be solved with both a numerical finite element approach and an analytical method was identified. The problem could involve just one or multiple physical fields. After solving the problem analytically, the problem was then modeled in COMSOL and solved using finite element analysis. The results of the finite element analysis were then compared to the analytical results to confirm the correctness of the numerical solution. To be able to solve them analytically, the problems usually involved a simple geometry. Performing the practice simulations was helpful in learning and demonstrating proficiency in the COMSOL software in preparation for replicating the published numerical simulations detailed later.

Several of the dominant physical fields involved in a lightning strike simulation are thermal

[1]This content is solely the responsibility of the authors and does not necessarily represent the views of the Institute for Computational and Data Sciences.

and electrical physics. A heat transfer problem that involves both thermal and electrical physics is Joule heating, or resistance heating, in a current-carrying wire. The surface temperature of the wire in a steady state was to be solved. The problem was defined fully so that the geometry was known, the current traveling through the wire was known, and the voltage drop across the length of the wire was known. The convection coefficient, ambient temperature, and thermal conductivity of the wire were also defined. With the problem stated, it was possible to obtain an analytical solution using equations provided in the textbook by Çengel [79]. After the analytical solution of the problem was found, the problem was modeled in COMSOL. The modeling process involves selecting the physics that are involved in the problem, specifying the type of study, creating the model geometry, configuring the physics, creating the mesh, running the simulation, and visualizing the results. The process is described in more detail for the replication work in the next section. For the Joule heating in a wire problem, the simulation was completed using the default mesh settings and then with a finer mesh to observe mesh convergence with comparison to the analytical results.

Several other practice simulations were performed. These included solving for the deflection of an axial bar under thermal stress, solving for the deflection of an orthotropic plate, and computing several configurations of fundamental beam mechanics problems. Performing these simulations in COMSOL helped to demonstrate knowledge of the features of the software and familiarity with navigating it. While not all physics explored were utilized in the replication and extension work detailed in the following sections, the work provided a more complete understanding of the capabilities of the software.

3.2 Study Replication

The work of Chen J. et al. presented experimental and numerical modeling of lightning strike components C and D on a CFRP composite laminate with a fastener, as introduced in Chapter 1. Their work allowed them to identify the different damage effects encountered in the composite and the fastener when exposed to the current components. More damage was observed to the fastener and less to the composite under current component C, and the opposite was observed under current component D [69]. This section describes first the experimental and numerical simulation details of the original study followed by the methods used to replicate the finite element simulations.

The experimental simulations of Chen J. et al. were performed on CFRP composite laminate specimens of unidirectional TC35/FRD-Y360 layers. The specimens were square with a side length of 250 mm and thickness of 2 mm. They consisted of 15 plies with a stacking sequence of $[0°/90°/0°/90°/0°/90°/0°/90°/0°/90°/0°/90°/0°/90°/0°]$. The fastener was fitted in a hole in the center of the specimen, was stainless steel in material, and was 8 mm in diameter. In the experimental tests, the lightning current was discharged into the fastener and exited out of all four sides of the composite specimen, which were grounded. The current waveforms applied were representative of lightning current components C and D. The experimental setup used by Chen J. et al. is shown in Fig. 3.1, which is from the original publication [69]. The positioning of the composite, the fastener, where the current is discharged, and the grounding can all be observed in the photograph.

In addition to their experimental tests, Chen J. et al. used finite element analysis in COMSOL

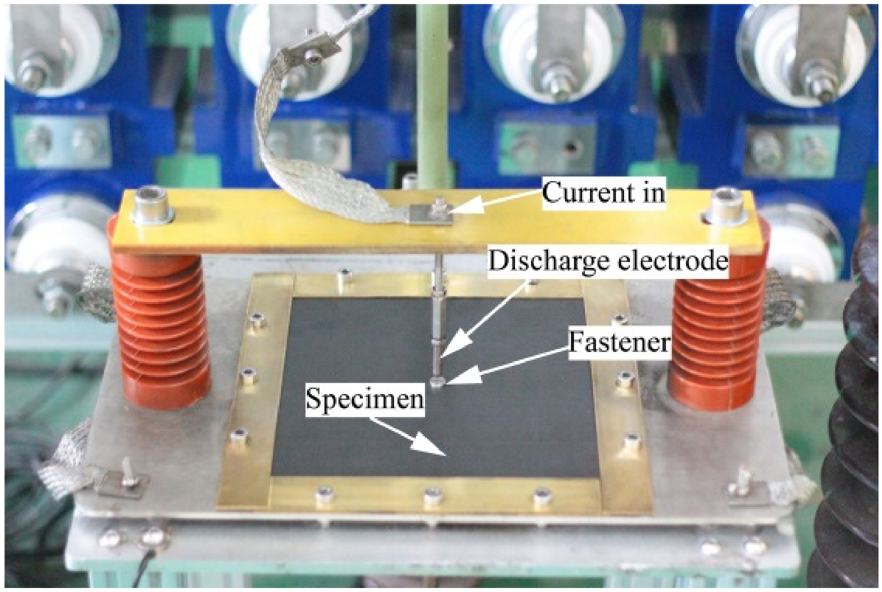

Figure 3.1: Experimental setup of Chen J. et al. [69].

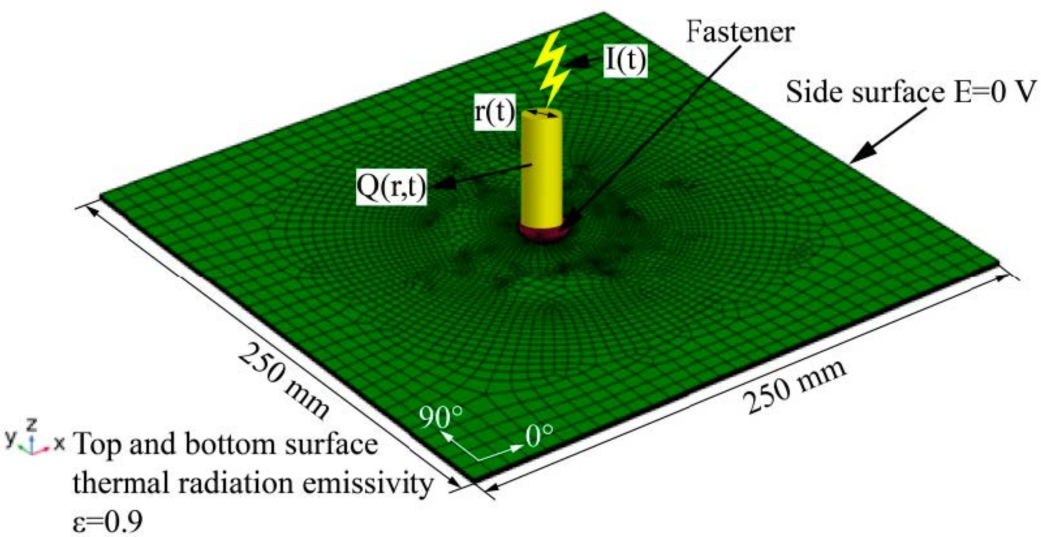

Figure 3.2: Finite element analysis model used by Chen J. et al. [69] showing geometry, boundary conditions, and mesh.

to model the simulated lightning strike. Their finite element analysis model is shown here in Fig. 3.2. The geometry and boundary conditions can be seen to match the experimental setup. They created six variations of the numerical model; three variations simulated lightning current component C, and three variations simulated lightning current component D. For each lightning current component, one variation has both applied electrical current and heat flux, one variation has only applied electrical current, and one variation has only applied heat flux. The creation of multiple variations of the model allowed for the influence of the electrical current and heat flux loads on damage to be evaluated for each current component. In their publication, Chen J. et al. presented a visual comparison of the damage obtained experimentally with ultrasonic scanning and the damage results from finite element analysis, which is shown here in Fig. 3.3. Additional details about their numerical simulations, some of which will be discussed shortly in explaining the replication methods used here, can be found in their publication [69].

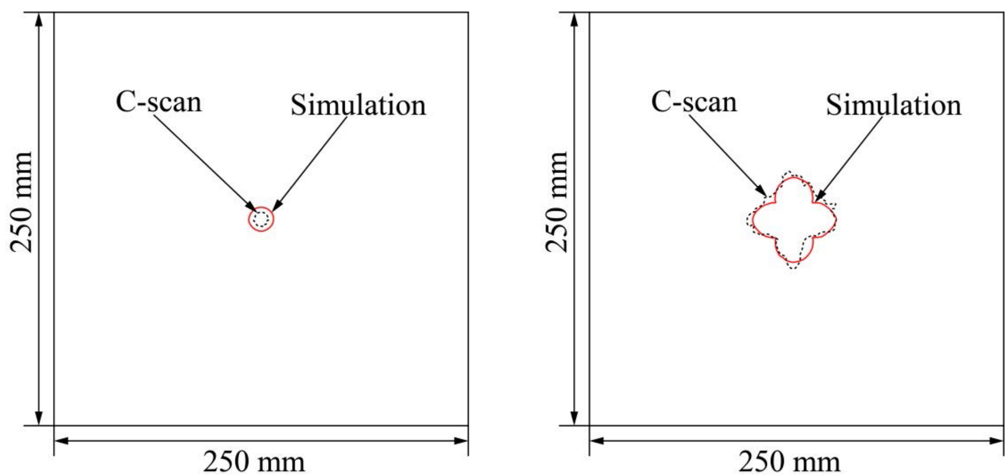

Figure 3.3: Comparison between experimental damage results and finite element analysis damage results for current component C (left) and current component D (right) from the work of Chen J. et al. [69].

To accomplish the replication work herein, the numerical simulation model of Chen J. et al. was closely studied with fine details being taken into account. Based on the information available, the six variations of the numerical simulation model were replicated in COMSOL. The first step in this process was selecting the space dimension, the physics involved, and the type of study. The simulation being replicated was performed in three dimensions and involved coupled thermal and electric physics. Therefore, `3D` was selected as the space dimension, and `Joule Heating` was selected for the physics, which adds the `Electric Currents`, `Heat Transfer in Solids`, and `Electromagnetic Heating` physics interfaces to the model. The lightning strike event is transient, so a `Time Dependent` study was selected. The next step was creating the geometry.

In COMSOL, the geometry was defined by first creating a work plane in the xy-plane of the global coordinate system. A square was defined with its center about the origin and with the specified side length. A circle was defined, which was also centered about the origin, to represent the fastener hole with the fastener diameter. The thickness of each ply was created using an extrusion, and an array was used to create the total 15 plies of the laminate. A separate work

Table 3.1: Material properties of the CFRP composite specimen used by Chen J. et al. [69] and in the replication model.

Temperature (°C)		25	300	500	510	3316	> 3316
Density $(\mathrm{kg/m^3})$		1472	1472	1110	1110	1110	1110
Specific Heat $(\mathrm{J/(kg \cdot K)})$		1176	2048	1454	1454	2146	5875
Thermal Conductivity $(\mathrm{W/(m \cdot K)})$	Longitudinal	6.578	9.617	7.166	7.166	7.166	1×10^8
	Transverse	0.723	0.633	0.423	0.423	0.423	1×10^8
	Through-Thickness	0.723	0.633	0.423	0.423	0.423	1×10^8
Electrical Conductivity $(\mathrm{S/m})$	Longitudinal	17 800	17 800	17 800	17 800	17 800	1×10^8
	Transverse	10.4	10.4	2000	2000	20 000	1×10^8
	Through-Thickness	2.8	2.8	2000	2000	20 000	1×10^8

plane, circle, and extrusion were used to create the domain of the fastener, which protruded slightly beyond the top and bottom surfaces of the laminate.

The next step involved adding material properties to the model, which were defined to match those used by Chen J. et al. [69]. Two materials were defined; one was defined for the composite laminate, and one was defined for the fastener. The material properties for the composite laminate are listed in Table 3.1. A rotated coordinate system was used to define the orientation of the material in the 90° plies with respect to the 0° plies. The 0° plies were aligned with the global coordinate system and, therefore, did not require rotation. `Interpolation` functions, built into COMSOL, were used to define the material properties of the composite that change with temperature. Within these functions, linear interpolation and constant extrapolation were used.

Defining the material properties of the stainless steel fastener required less work as the properties used by Chen J. et al. do not vary with temperature. The fastener is also isotropic, which means it only has one defining value each for electrical conductivity and thermal conductivity [69]. The material properties of the fastener are shown in Table 3.2.

Following the assignment of the material properties, the boundary conditions were added to the model. The composite laminate is grounded on its four sides. Therefore, a boundary condition was defined in that the electric potential of the four sides is set to zero. For convenience, in the `Electric Currents` interface, COMSOL includes `Ground`, which sets the zero-electric potential boundary condition to the boundaries that are selected. As in the work of Chen J. et al. [69], thermal radiation was specified for the top and bottom surfaces of the laminate with an emissivity of 0.9. The ambient temperature in the model was 25°C or 298.15 K, following that which was used by Chen J. et al. [69]. The model reference temperature and initial temperature were also set to 25°C for consistency.

Table 3.2: Material properties of the stainless steel fastener used by Chen J. et al. [69] and in the replication model.

Density $(\mathrm{kg/m^3})$	7850
Specific Heat $(\mathrm{J/(kg \cdot K)})$	475
Thermal Conductivity $(\mathrm{W/(m \cdot K)})$	44.5
Electrical Conductivity $(\mathrm{S/m})$	4.032×10^6

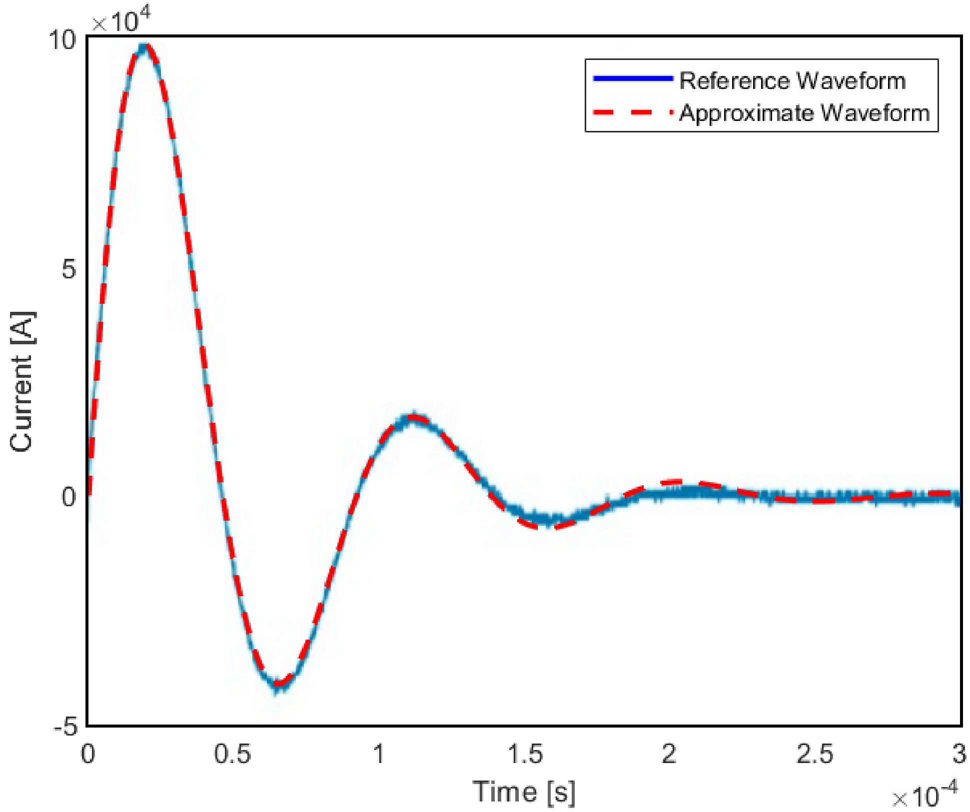

Figure 3.4: Approximate waveform developed for current component D superimposed over waveform data used by Chen J. et al. [69].

Next, the loads were defined. The loads varied depending on the current component being applied and whether the model variation included the application of electric current, heat flux, or both. In the work of Chen J. et al., the lightning current waveforms were imported into COMSOL for use in applying the loads [69]. However, while graphs of the data are shown in their publication, the exact data is not available. Therefore, approximations were made here for both current component C and current component D. Current component C was modeled with a constant applied load of 200 A for the duration of 1 s. Current component D was modeled with a decaying sinusoidal expression representative of the experimental waveform plot, the peak amplitude, and the action integral of Chen J. et al. [69]. The expression was developed by superimposing the resulting plot over the experimental waveform and by calculating the peak amplitude and action integral. The process was performed in MATLAB and involved manual adjustment of the expression parameters until the values of peak amplitude and action integral and the plotted waveform closely matched those of Chen J. et al. Equation (3.1) is the developed expression, and the superimposed waveform plot is shown in Fig. 3.4.

$$I\left(t\right) = ae^{-bt}\sin\left(ct\right) \tag{3.1}$$

Variable I represents the current with respect to time, t. Parameters a, b, and c have values of 1.470×10^5 A, 1.897×10^4, and 6.803×10^4, respectively. The expression for current component D was defined in COMSOL as an `Analytic` function and used to define the applied current. Heat flux was modeled as a function of the current, following Eq. (3.2), as done by Chen J. et al. [69].

$$Q\left(r,t\right)\approx 10J\left(r,t\right) \tag{3.2}$$

Here, Q is the heat flux, J is the normal current density, and r is the radial distance from the center of the fastener. The normal current density is a function of the current, I, over the surface area of the top of the fastener. In the model variations with both electric current and heat flux loads, both Q and J were applied to the top surface of the fastener geometry. In the model variations with only electric current, only J was applied. In the model variations with only heat flux, only Q was applied. In this study, the current density is uniform over the fastener, meaning that J and Q do not change with r over the surface applied. With the application of electric current, heat flux, or both, the boundary conditions were fully defined.

After applying the boundary conditions, it was necessary to define the mesh. Chen J. et al. reports having used a total of 28,157 elements for their model [69]. While some additional details of the mesh are provided, the complete specifications of the mesh they used are not known. To best replicate their simulation, a user-generated mesh was chosen for the model. The mesh was created by first defining a two-dimensional quadrilateral mesh for the top surface of the geometry using the `Free Quad` operation and then by sweeping the two-dimensional mesh through the volume of the geometry using the `Swept` operation.

Since the exact mesh used by Chen J. et al. is not known, it was important to demonstrate mesh convergence, which is a process discussed in the previous chapter. One of the important measured results in the study is the size of the decomposition damage region, which was determined to be the region that exceeds 300°C [69]. Chen J. et al. found that this region extends in the direction of the fibers and measured the length of the region in the same direction [69]. Therefore, for the work here, the length of the decomposition damage region in the first layer was measured for each iteration of mesh refinement. The model variation including current component D and both applied electric current and heat flux was used. The damage length values were plotted to show convergence of the model results. This is shown in Fig. 3.5.

While the convergence plot does not show a smooth transition, attention should be focused on the differences between consecutive iterations, which are small. Beyond approximately 4,000 domain elements, the difference is less than 1 mm. When compared to the average damage length observed under current component D with combined applied electric current and heat flux, the difference of 1 mm is only about 2%. For predicting the size of the damage region in the composite, this was determined to be an acceptable deviation. For increased refinement of the mesh, particularly around the fastener, the most refined mesh used in the mesh convergence test was used for the model. This mesh consisted of 11,719 domain elements. While it did require more computational resources than meshes with fewer elements, this mesh provided greater resolution around the fastener.

The last step of establishing the model was defining the settings for the transient solver. The simulations were computed for a total time interval corresponding to the duration of each respective current component. The analyses for current component C were computed for a total time interval of 1 s while those for current component D were computed for a total time interval of 300 μs, matching the time intervals used by Chen J. et al. [69]. To allow for visualization of

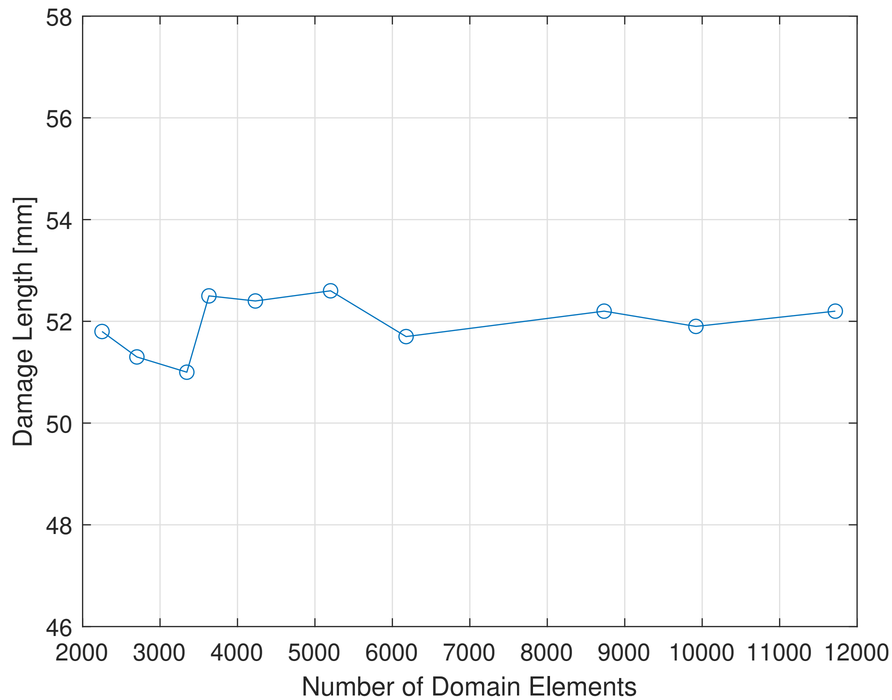

Figure 3.5: Mesh convergence plot for the replication model that shows small differences between consecutive meshing iterations above approximately 4,000 domain elements.

results over time but not demand unnecessary resources, data for ten equally-spaced time increments were stored for each simulation. This is not to be confused with the timesteps that are used to solve the system; COMSOL automatically decides on timestep size based on the requirements of the solver. The same relative tolerance of 0.01 was used for the transient solver as that which was used by Chen J. et al. [69].

With the geometry, boundary conditions, mesh, and solver settings defined, the model was now complete. The model is summarized visually in Fig. 3.6. The model could be adjusted to include applied electric current, applied heat flux, or both under either current component C or current component D. Simulations were run for each of the six variations of the model, and results were collected. The computation time for the simulations varied greatly with the shortest computations only taking several minutes and the longest taking over 13 hours. The longest computation times were required by the variations of the model that included applied electric current under current component D. The results of the simulations, including descriptions of how they were visualized, are presented in Chapter 4.

3.3 Study Extensions

As mentioned in Chapter 1, the traditional method of LSP for CFRP composites is the application of a conductive, metallic mesh on the outer layer [2]. Instead of forcing the electric current of the lightning strike to travel through the CFRP and cause damage, the metallic mesh

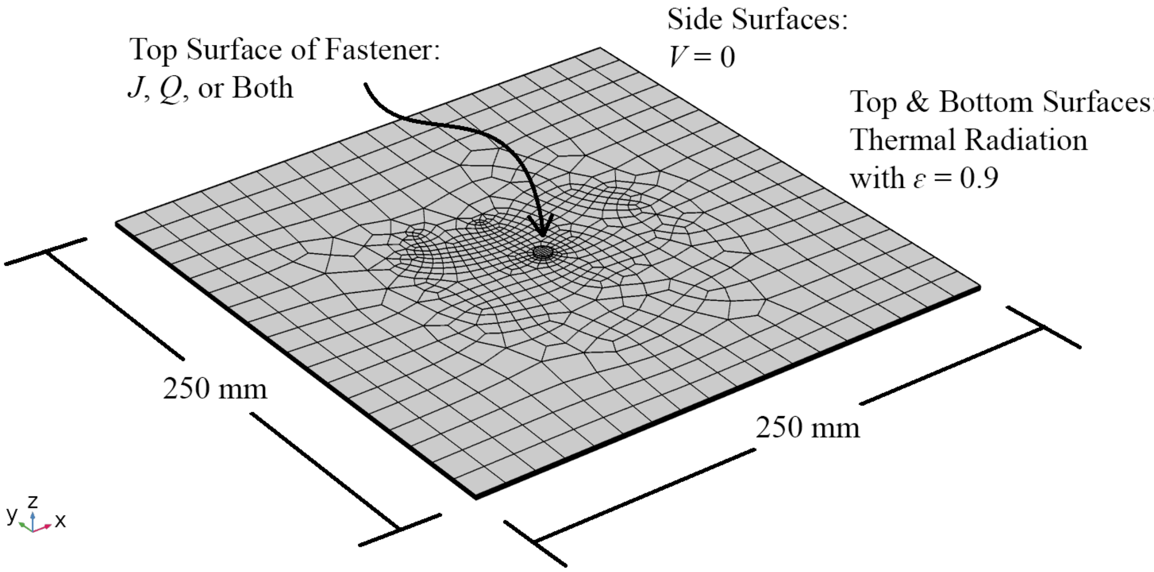

Figure 3.6: Geometry, boundary conditions, and mesh used in the replication model.

provides an alternative path of conductivity for the electric current to travel. The application of a metallic mesh has been modeled for simulation by finite element analysis by several researchers [21, 51, 62, 70, 71]. These studies involved detailed modeling of the metallic mesh and the assignment of transient material properties. The extension work performed herein involved examining the effects of adding a solid copper outer layer to the model and also the effects of using different stacking sequences.

Several assumptions were made in the application of the copper layer. The layer was assumed to be a single, homogeneous domain with length and width dimensions matching those of the CFRP composite specimen. The layer was also assumed to behave with static material properties, similar to those used for the fastener. These assumptions allowed for decreased computation time while still demonstrating the general effects of the addition of a copper layer. The copper layer geometry was added to the simulation model on the top side of the laminate by using an extrusion and defining the thickness. The side boundaries of the copper layer were grounded, and the thermal radiation boundary condition with emmissivity of 0.9 for the top layer was moved from the top of the CFRP specimen domain to the top of the copper layer domain. The copper layer was defined using the material properties shown in Table 3.3, which are built-in material properties available in COMSOL.

Table 3.3: Material properties of copper used in the addition of a copper outer layer.

Density $(\mathrm{kg/m^3})$	8960
Specific Heat $(\mathrm{J/(kg \cdot K)})$	385
Thermal Conductivity $(\mathrm{W/(m \cdot K)})$	400
Electrical Conductivity $(\mathrm{S/m})$	59.98×10^6

With the addition of the copper layer, different thicknesses of the copper layer were tested. Thicknesses tested ranged from 0.005 mm to 0.12 mm for current component C and 0.02 mm to

0.12 mm for current component D. Simulations were performed using the variation of the replication model that includes both applied electric current and applied heat flux. The same transient solver settings were used as in the replication model. A mesh consisting of 10,576 domain elements was used for all tested thicknesses except 0.01 mm and 0.005 mm, which both required a finer mesh to allow for convergence. For these, a mesh including 32,408 domain elements was used. Once the model was set up, simulations were run for each thickness of the copper layer and lightning current component, and results were collected.

Aside from the implementation of the copper layer, further exploration was performed based on the replication model by making variations of the model with different laminate stacking sequences. This was done for current component D with both electric current and heat flux applied because the largest decomposition damage regions in the replication model were observed under current component D. The original stacking sequence was bi-directional and followed that which was used by Chen J. et al. [69]. The alternative stacking sequences tested are shown in Table 3.4. The first alternative stacking sequence has 45° and -45° plies separated by 0° plies and was selected because it involves three fiber orientations compared to the original replication model that involves two. The second alternative stacking sequence has 45°, 0°, -45°, and 90° plies. It has 16 plies instead of the original 15 of the replication model. In the model using the second alternative stacking sequence, the layer thickness was reduced so that the overall thickness of the laminate was not changed. The second alternative stacking sequence was selected because it involves four different fiber orientations as well as symmetry. After performing the extension work simulations, the results were visualized and are presented in Chapter 4.

Table 3.4: Stacking sequences tested under current component D for comparison of damage results.

Test	Stacking Sequence	Plies
Original	$[0°/90°/0°/90°/0°/90°/0°/90°/0°/90°/0°/90°/0°/90°/0°]$	15
1	$[0°/45°/0°/-45°/0°/45°/0°/-45°/0°/45°/0°/-45°/0°/45°/0°]$	15
2	$[45°/0°/-45°/90°]_{2S}$	16

Chapter 4

Results

Previously, in Chapter 3, the methods used to set up and perform the finite element simulations were discussed. Here, the results obtained from the simulations are presented. First, the results of the replication of the simulations of Chen J. et al. are shown with comparisons made between the published results of Chen J. et al. and the replication model. Next, the results of the study extensions, which include the addition of a copper outer layer and using different stacking sequences, are presented.

4.1 Study Replication

In Chapter 3, the methods of the study of Chen J. et al. and those used to replicate their numerical simulations were discussed. The goal of the numerical simulations in the work of Chen J. et al. was to simulate the lightning strike damage in the CFRP composite laminate to allow for closer analysis of the complex event. To do this, the simulated temperature of the CFRP composite was analyzed to identify regions that exceeded the decomposition temperature of 300°C. Using temperature contours, the researchers were able to visualize the decomposition damage and compare it to their experimental results. They found agreement between the decomposition damage identified in their experiments and that which was predicted by the finite element simulation [69]. To validate the replication of the model of Chen J. et al., the work herein involved visualizing the regions of decomposition damage and preparing the results for comparison with the results of Chen J. et al.

To compare the model developed herein to that of Chen J. et al., it was necessary to properly configure the visualization of the simulation results. Like similar commercial finite element software, COMSOL has the built-in functionality of visualizing simulation results. To visualize the temperature results of multiple layers of the composite laminate, the visualization feature `Slice` was used, which presents the values of a specified output variable in one or multiple planes of the geometry. In this case, the desired output variable was temperature. The feature was used to visualize in-plane, or xy-plane, temperature results at the midpoint of the thickness of each lamina. To only show the area of decomposition damage, a data range minimum of 300°C was applied. The temperature contour was set to also have a minimum of 300°C. The maximum of the contour was set to 3316°C for most cases. In the model variation with electric current only under current component C and the model variation with heat flux only under current component D, the maximum temperatures were much less than 3316°C, so the contour maximums in these cases were left at the default settings. By default, COMSOL sets the contour maximum to the maximum of the data (*i.e.*, temperature). Images of the temperature contours of the top four laminae were superimposed in post-processing with each made 50% transparent. The top surface of the fastener is included in each superimposed plot as well. Length measurements of the decomposition damage region were taken from the top two laminae to the nearest tenth of a millimeter. The in-plane results for current component C are shown in Fig. 4.1, and the in-plane results for current component D are shown in Fig. 4.2.

Following the visualization of the in-plane, or xy-plane, temperature results, the temperature results in the thickness direction of the laminate in the xz-plane were collected. This visualization also involved the use of the `Slice` feature. Now, the plane displayed was the xz-plane at the center of the laminate, which allowed for the temperature through the thickness of both the fastener and the laminate to be visualized. No data range minimum was set for this visualization. The temperature contour range was set to have a minimum of 300°C. The contour maximum was set to either 3316°C or left at the default. The through-thickness temperature results for current component C and current component D are shown in Fig. 4.3 and Fig. 4.4, respectively. All replication model results were collected from the final time increment of the transient study.

Beginning with the in-plane temperature results, it can be observed in Fig. 4.1 and Fig. 4.2 that there is good agreement in both the shape and size of the decomposition damage region predicted by the model of Chen J. et al. and the replication model developed herein for all six model variations. The differences that do exist between the two sets of results are between decomposition damage length measurements and some temperature values. The largest difference in decomposition damage length is 2.1 mm in the model variation with current component D and only electric current applied. This difference is approximately 4.19% of the damage length of 50.1 mm found by Chen J. et al. The possible reasons for the differences between the results will be discussed in Chapter 5.

With current component C, the damage decomposition region in the CFRP composite is centered about the fastener and is circular in shape. The fastener experiences higher temperatures than the CFRP composite when heat flux is applied in the model. The size of the decomposition damage reaches a fuller extent when electric current is applied compared to when only heat flux is applied. When both loads are applied, the largest decomposition damage size is observed.

With current component D, the damage decomposition region in the CFRP composite is centered about the fastener but extends outward in the direction of the fibers of the CFRP composite. A decomposition damage region is only observed when electric current is applied. When only heat flux is applied, only the fastener experiences temperatures greater than 300°C. However, when only electric current was applied, the temperature in the fastener did not rise above 300°C.

Next, the temperature results in the direction of the laminate thickness, or the xz-plane, which are shown in Fig. 4.3 and Fig. 4.4, are presented. Similar to the in-plane temperature results, there

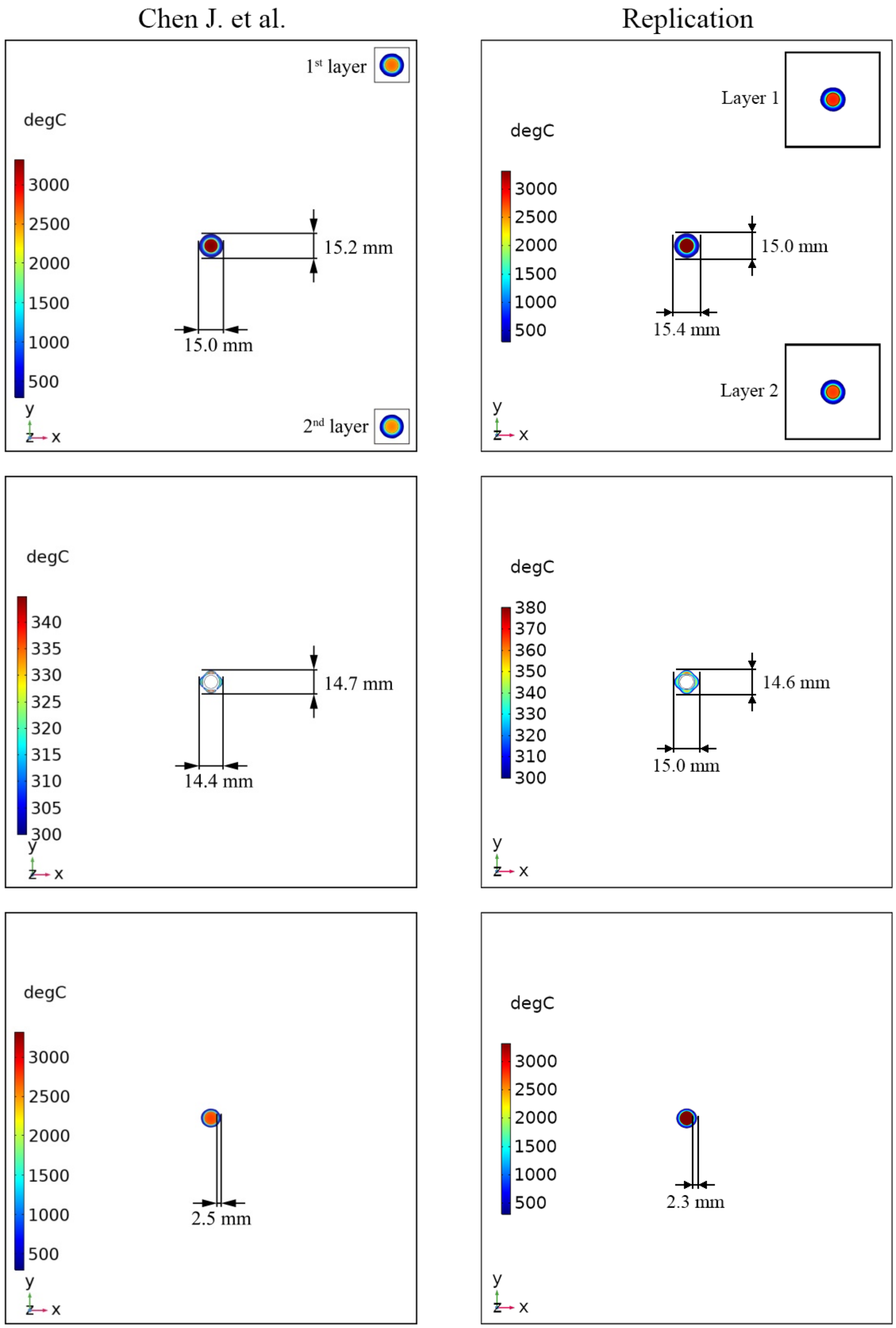

Figure 4.1: Comparison of in-plane results for current component C from the work of Chen J. et al. (left) [69] and the replication model (right). From top to bottom, the rows correspond to combined electric current and heat flux, electric current only, and heat flux only.

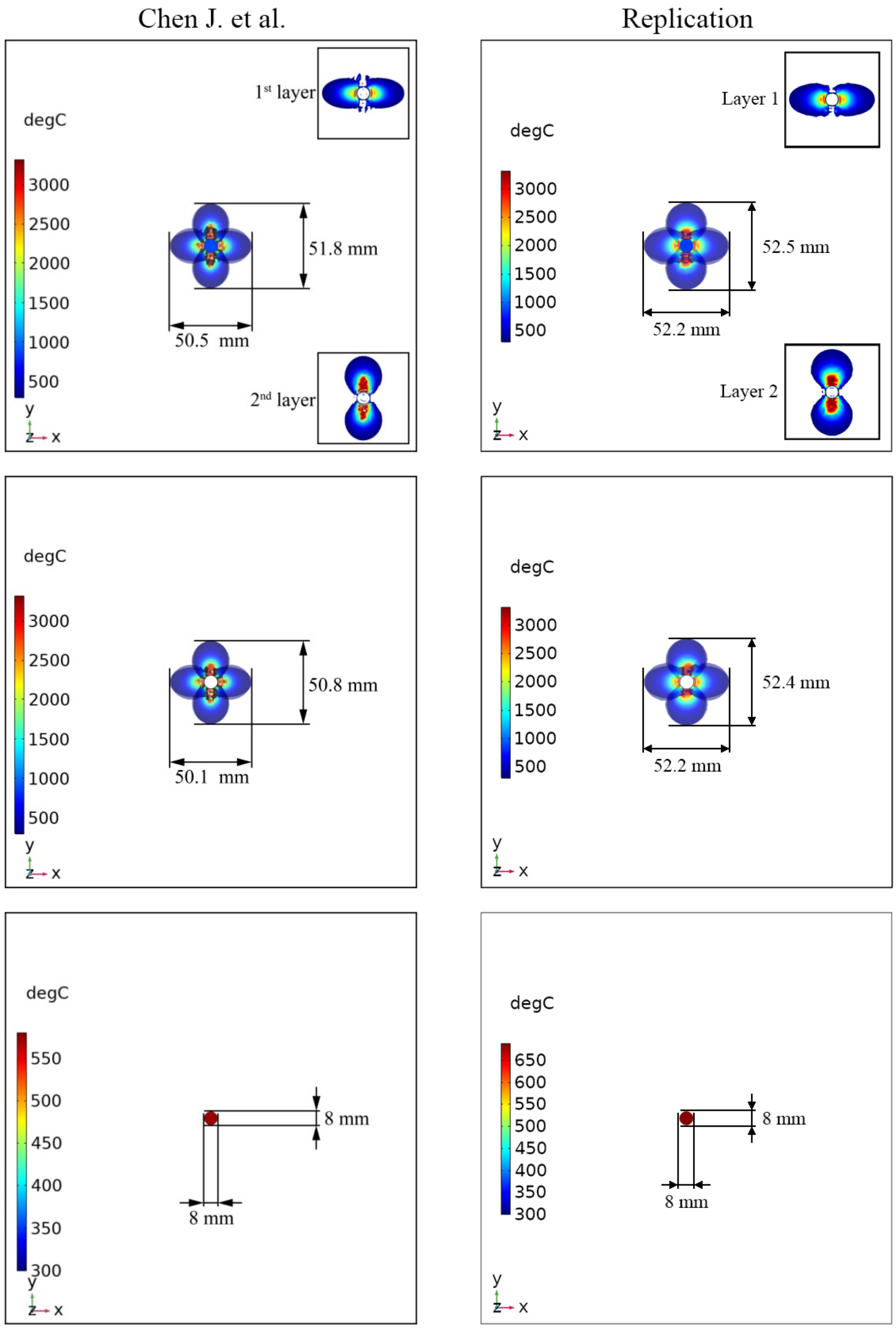

Figure 4.2: Comparison of in-plane results for current component D from the work of Chen J. et al. (left) [69] and the replication model (right). From top to bottom, the rows correspond to combined electric current and heat flux, electric current only, and heat flux only.

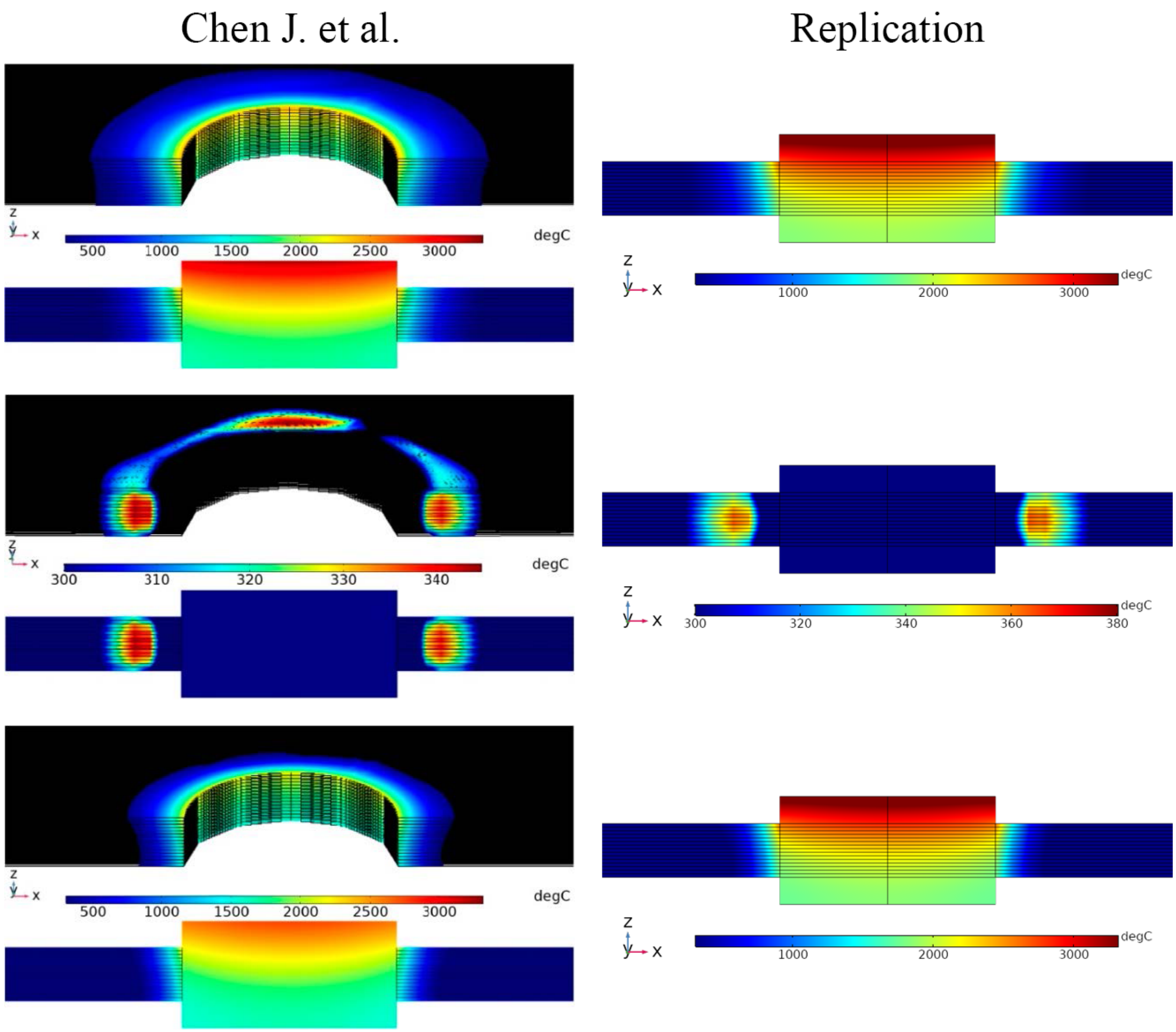

Figure 4.3: Comparison of through-thickness temperature results in the xz-plane for current component C from the work of Chen J. et al. (left) [69] and the replication model (right). From top to bottom, the rows correspond to combined electric current and heat flux, electric current only, and heat flux only.

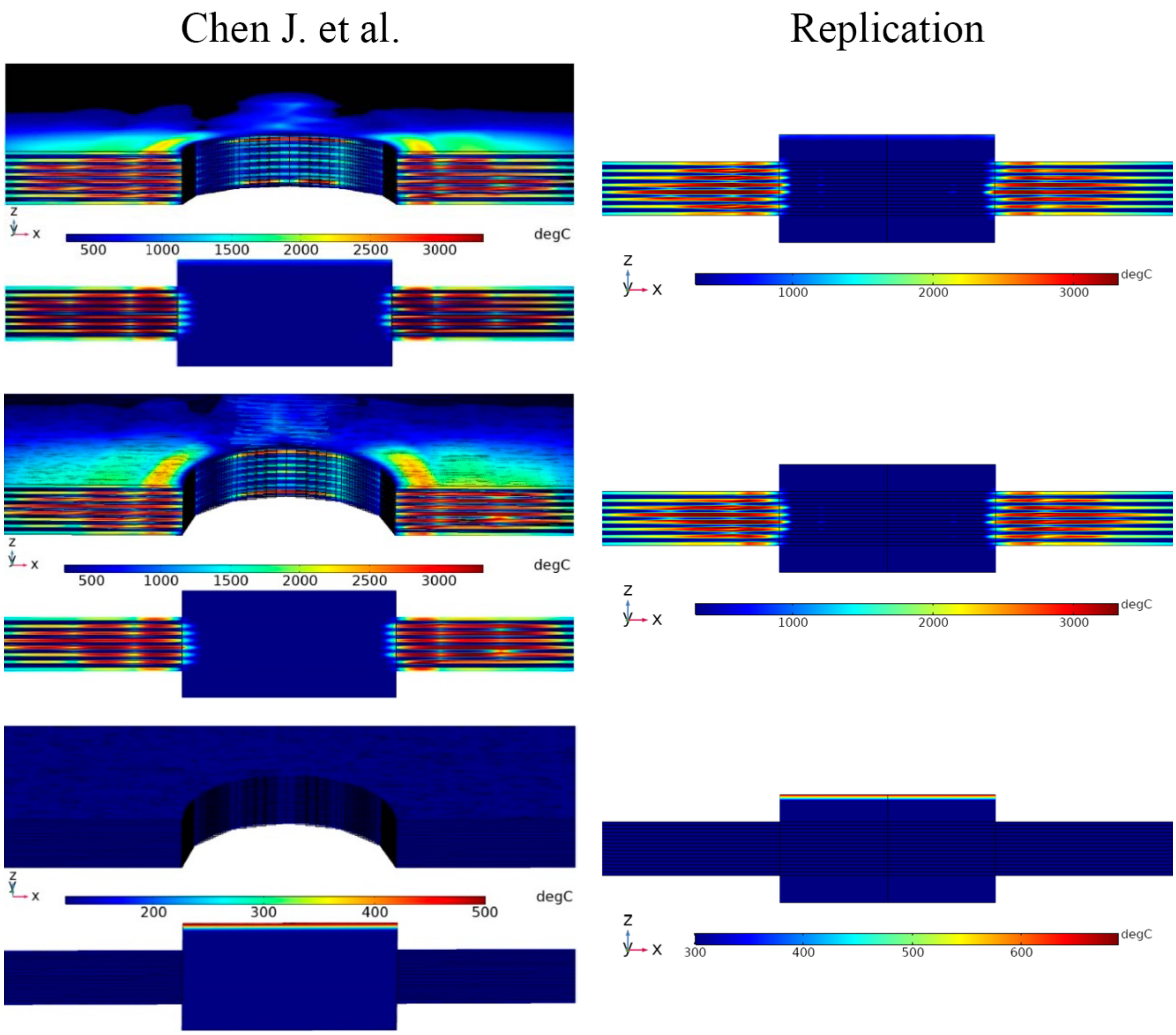

Figure 4.4: Comparison of through-thickness temperature results in the xz-plane for current component D from the work of Chen J. et al. (left) [69] and the replication model (right). From top to bottom, the rows correspond to combined electric current and heat flux, electric current only, and heat flux only.

is good agreement shown between the xz-plane temperature results of the model of Chen J. et al. and the results of the replication model developed herein. Overall, the temperature distributions in the fastener and laminae between the two sets of results match closely. The only apparent differences between the two sets of results are small differences between the temperature distributions and possibly some different maximum temperature values. Similar to the in-plane results, the possible reasons for these differences will be discussed in Chapter 5.

The view of the xz-plane with current component C shows that the applied heat flux caused the most significant rise in temperature in the fastener, and some of the heat was transferred to the surrounding CFRP composite. In contrast, the applied electric current had less of an impact on the temperature of the fastener but instead caused some heating in the CFRP composite at a greater distance from the fastener.

In the view with current component D, the heating effects caused by the applied electric current are present throughout the thickness of the laminate. Differences in temperature between layers depending on fiber orientation are observed, which agrees with the in-plane temperature results. The effect of the applied heat flux was mostly contained to the top of the fastener and did not lead to temperatures as high as with the applied electric current.

4.2 Study Extensions

The first of the extension work performed herein involved adding a copper layer of varied thickness to the top of the CFRP composite laminate in the model. For analysis and comparison of testing different thicknesses, the maximum temperature produced in the domain of the CFRP composite during the simulation was recorded. The built-in `Volume Maximum` feature in COMSOL was used to evaluate the maximum temperature in the volume of the CFRP composite at all recorded time increments of the simulation. For current component C, the maximum temperature always occurred at the final time increment. For current component D, the maximum temperature generally occurred between 60 µs and 120 µs. The overall maximums were recorded and then plotted with respect to copper layer thickness for the corresponding current component. The results for current component C are shown in Fig. 4.5, and the results for current component D are shown in Fig. 4.6. In the plots, zero thickness refers to the original model that does not have the copper layer added, for which the maximum temperature was also collected.

The results of adding the copper layer show that, for both current components, the maximum temperature in the CFRP composite was reduced. Under current component C, the maximum temperature was reduced from 2745.3°C with no copper layer to 1760.0°C with the thickest copper layer tested of 0.12 mm. Under current component D, the maximum temperature was reduced from 4529.9°C without a copper layer to 197.13°C with the 0.12-mm-thick copper layer. The reduction in maximum temperature between no copper layer and the thickest copper layer tested was greatest under current component D.

In addition to collecting the maximum temperature in the CFRP composite, the `Slice` visualization feature was used to produce temperature contour plots of the top surface of the laminate. These plots are included here in Fig. 4.7. Similar to previous temperature results, a data minimum of 300°C was set to match the decomposition temperature. The minimum and maximum of the temperature contour were set to 300°C and 3316°C, respectively. The results were collected from the simulation time increment at which the maximum temperature in the

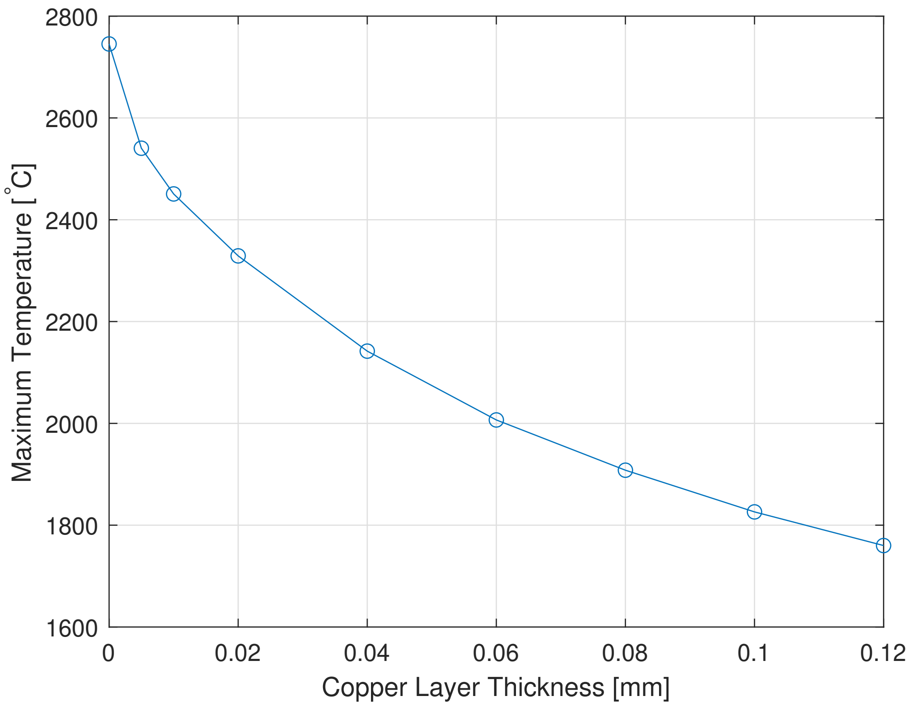

Figure 4.5: Maximum temperature in CFRP composite with respect to copper layer thickness under current component C.

volume of the laminate was observed. The results show that, under current component C, while the maximum temperature decreases with increasing copper layer thickness, the size of the decomposition damage region on the top surface increases. Under current component D, the decomposition damage region decreases in size with increase in copper layer thickness. Only the outline of the fastener geometry is shown for current component D with the 0.12-mm-thick copper layer. No temperature contour is visible as the maximum temperature in this case did not exceed the decomposition temperature of 300°C.

Separate from simulating the addition of a copper outer layer, different stacking sequences for the CFRP composite laminate were tested. The original model featured a bi-directional stacking sequence that alternated between 0° and 90° fiber directions. The different stacking sequences tested involved one with alternating 45° and -45° plies with 0° plies in-between and a second with a repeated and symmetric sequence of 45°, 0°, -45°, and 90° plies. The alternative stacking sequences and their respective notation were detailed in the previous chapter in Table 3.4. After the new model variations were set up and run in COMSOL, the in-plane temperature results were collected using similar visualization techniques to the results of the original replication model. All results were collected from the final time increment of the simulations.

The results for the first alternative stacking sequence that was tested are shown in Fig. 4.8. The `Slice` feature in COMSOL was used to visualize the temperature contour in the xy-plane at the midpoint of the thickness of each of the top four layers of the laminate. The data minimum was set to 300°C, and the contour minimum and maximum were set to 300°C and 3316°C, respectively. Images of the top four layers were superimposed and are shown on the left in the

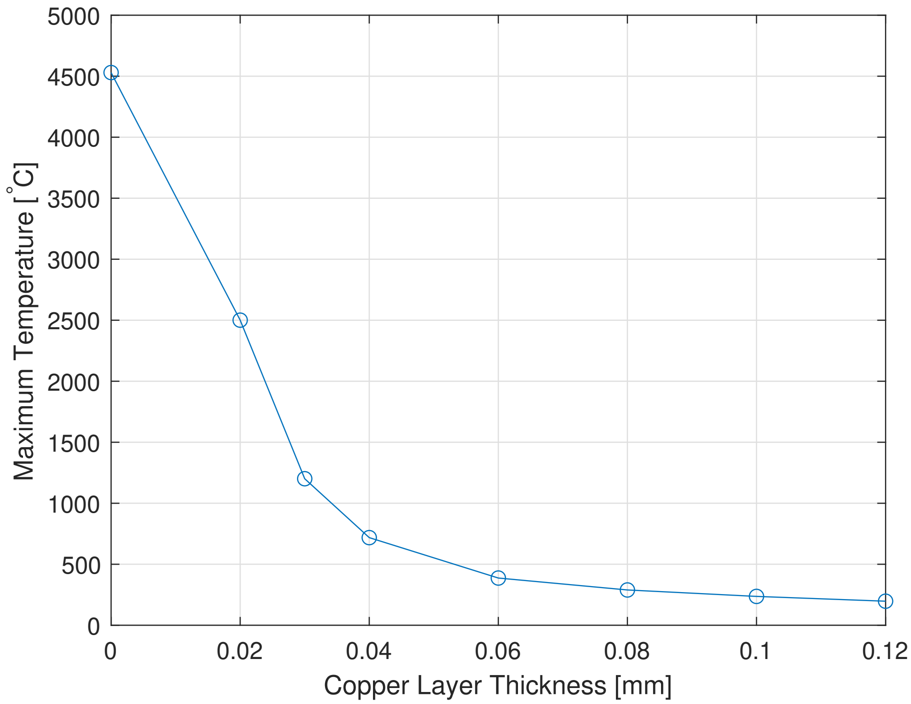

Figure 4.6: Maximum temperature in CFRP composite with respect to copper layer thickness under current component D.

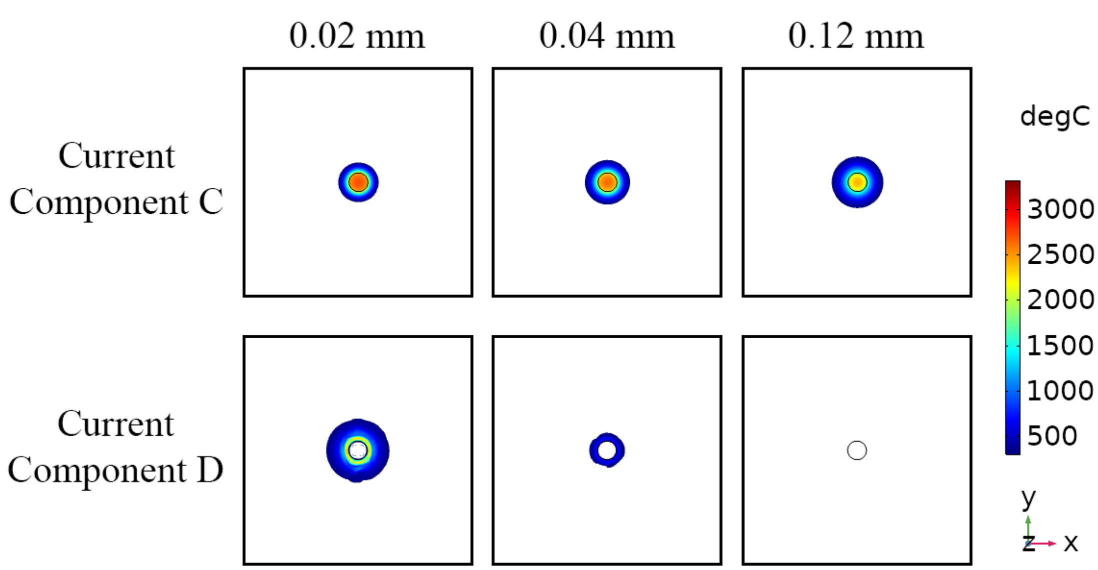

Figure 4.7: In-plane decomposition damage results on top surface of laminate for three different copper layer thicknesses subjected to the two current components.

figure, and they are also shown individually on the right. The temperature of the top surface of the fastener was also included in the superimposed plot. It can be observed that the decomposition damage is centered about the fastener and that the length of the decomposition damage is oriented in the same direction as the fibers in all layers observed. In the first and third layers, the decomposition damage travels along the x-axis, which corresponds to the 0° fiber orientations. The decomposition damage in the second layer and fourth layer extends 45° and -45°, respectively, from the positive and negative x-directions, which also correspond to the respective fiber orientations. The superimposed temperature contours show that the damage through the thickness of the laminate is roughly rectangular in shape. The length of decomposition damage in the x-direction is 60.2 mm while the length in the y-direction is 49.0 mm.

The results for the second alternative stacking sequence are shown in Fig. 4.9. Similar visualization procedures to the first alternative stacking sequence were used, including the same data and contour range settings. Like the first alternative stacking sequence, the decomposition damage extends outward from the fastener in the direction of the fibers. The decomposition damage is visualized in layers 1 through 4 with fiber orientations of 45°, 0°, -45°, and 90°, respectively. It was found that the largest length of decomposition damage in the y-direction was present in the 8^{th} and 9^{th} plies, which exhibited nearly identical decomposition damage regions. Layers 8 and 9 are the two layers about which the symmetry of the stacking sequence occurs, and the two layers are also included individually in Fig. 4.9. The superimposed temperature contours show that the damage through the laminate thickness is roughly circular in shape. The decomposition damage length in the x-direction was 54.6 mm. The decomposition damage length in the y-direction was 56.4 mm and was found in layers 8 and 9.

Between the two alternative stacking sequences tested, the largest decomposition damage length found was 60.2 mm in the x-direction of alternative stacking sequence 1. The largest damage length of the original stacking sequence under current component D was 52.5 mm in the y-direction. Therefore, the largest decomposition damage length found with an alternative stacking sequence is approximately 14.7% greater than the largest damage length of the original stacking sequence. The findings of the study extensions will be discussed in Chapter 5.

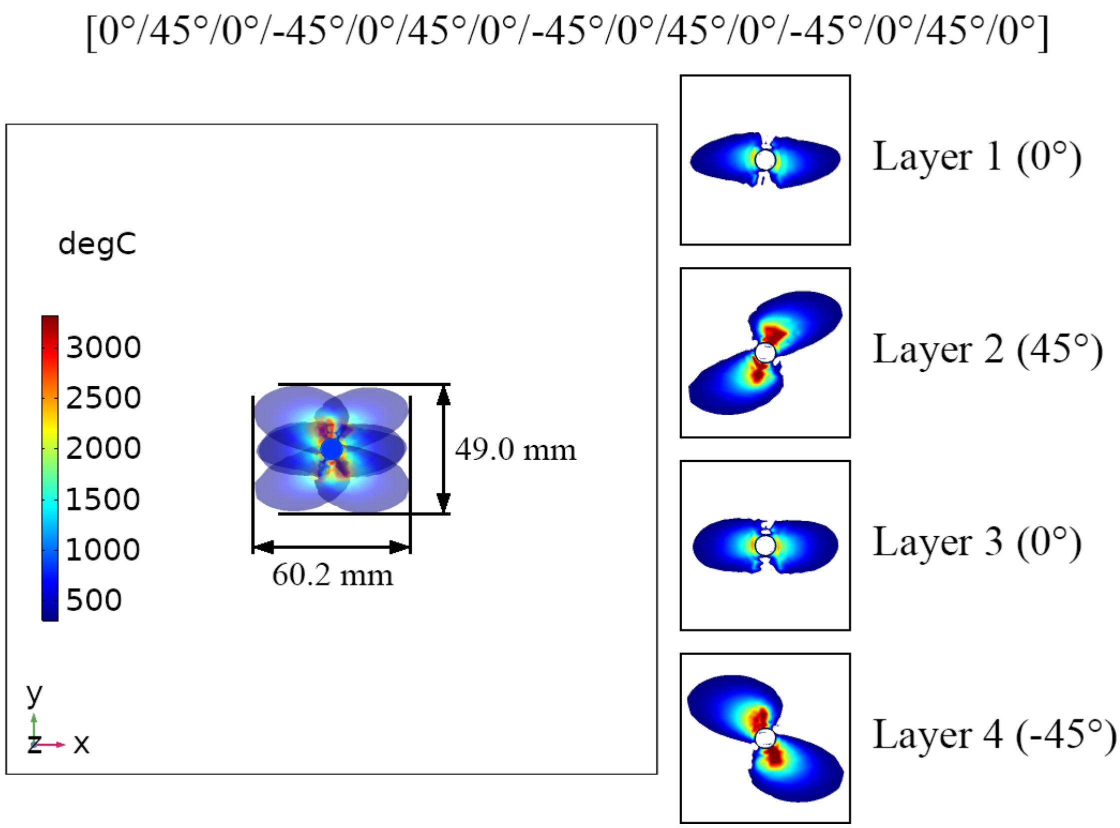

Figure 4.8: Temperature contours superimposed and by layer for alternative stacking sequence 1 under current component D.

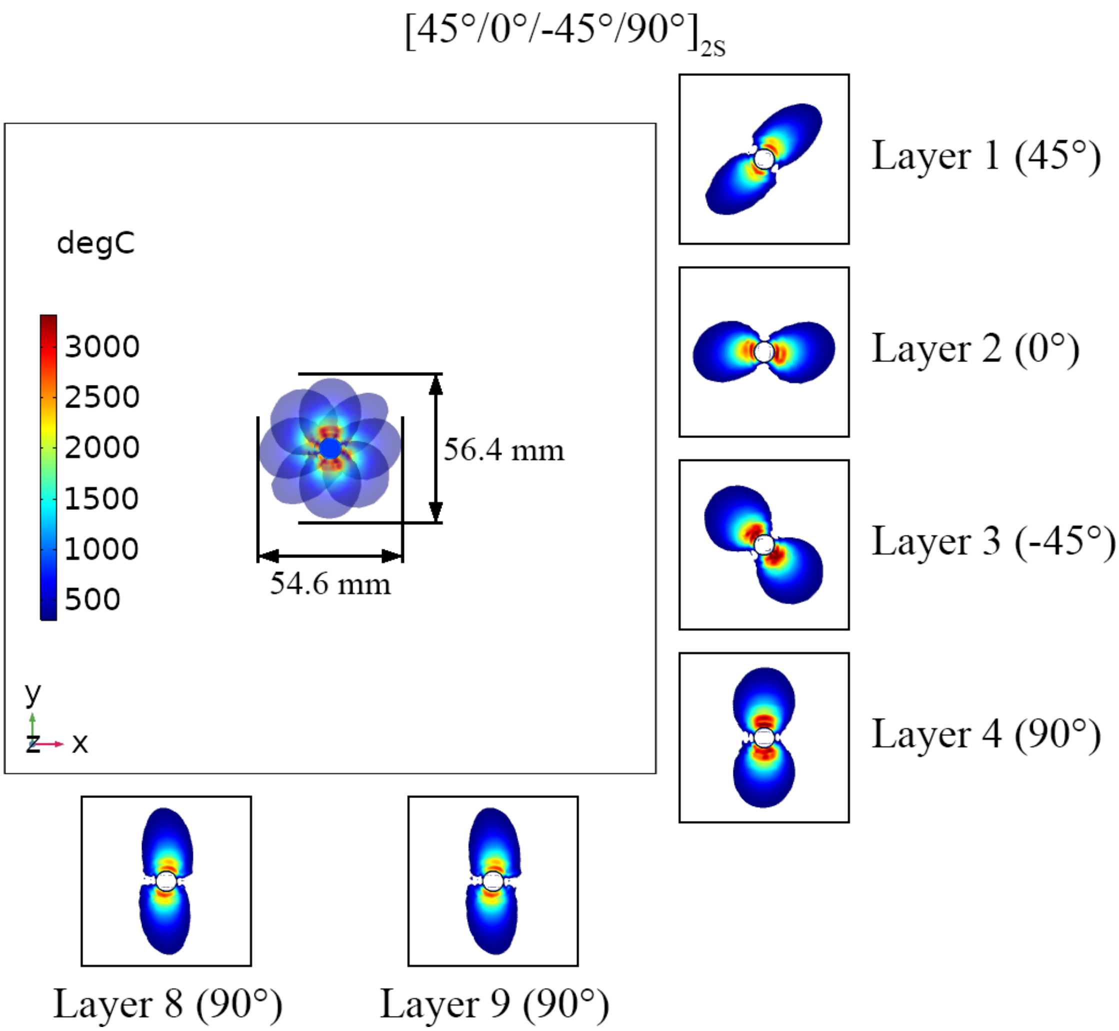

Figure 4.9: Temperature contours superimposed and by layer for alternative stacking sequence 2 under current component D.

Chapter 5

Discussion

Here, the results that were presented in Chapter 4 are discussed. The results of the replication model and their comparison to the results of Chen J. et al. are discussed first. The similarities and differences between the two sets of results are analyzed, and possible explanations for the differences are given. Next, the results of the study extensions are visited, which include adding a copper outer layer and varying the laminate stacking sequence.

5.1 Study Replication

Comparing the original results of Chen J. et al. and the results of the replication model is critical in assessing whether the original model was replicated accurately. The comparison was presented in Chapter 4 in Section 4.1, and it was categorized by visualization and lightning current component. The comparisons for the xy-plane, or in-plane, view for current components C and D were shown in Fig. 4.1 and Fig. 4.2, respectively. The comparisons for the xz-plane view for current components C and D were shown in Fig. 4.3 and Fig. 4.4, respectively. Through these listed comparisons, good agreement was found between the original results of Chen J. et al. and the results of the replication model for all model variations.

Following what was done by Chen J. et al., the replication work herein involved the creation of six variations of the lightning simulation model. In each comparison of in-plane decomposition damage results, the findings of the shape of the decomposition damage of the replication study closely match those of Chen J. et al. There are small differences in the decomposition damage lengths and some temperatures. The largest length difference is 2.1 mm, which was found between the results in the x-direction of the model variation with current component D and only electric current applied, shown in Fig. 4.2. In this case, the damage length found by the replication model is 4.19$\%$ greater than that found by the published model. It is reasonable that the largest difference was observed in one of the model variations that exhibited the largest decomposition damage lengths. The difference does not negatively impact the usefulness of the result in predicting decomposition damage. The discrepancy would be a greater concern if it was observed in any of the model variations with current component C, for example, which demonstrated smaller regions of decomposition damage. However, the differences in the cases of current component C are smaller. In each comparison of xz-plane results, the plots obtained through the replication study also closely match those of Chen J. et al. Similarly, there are some small differences in temperatures.

The reasons for the differences between the results of the replication work and the results of Chen J. et al. are likely due to differences in modeling and visualization techniques. The differences start with the methods used to set up the model, which were described in Sec. 3.2. In the replication model, the lightning current waveforms were approximations of the data used by Chen J. et al. A different mesh was used in the replication model than by Chen J. et al. The exact visualization techniques used by Chen J. et al. are not known. The visualization techniques used to present the results of the replication model were selected because they appear to be the most similar to those used by Chen J. et al. However, differences in visualization techniques may be present. For example, it is possible that Chen J. et al. presented results from different or all layers or different time increments. While differences are present between the two models, the differences do not appear to be significant enough to cause issues with the accuracy of the replication model. It can be stated that the replication model developed in this study is capable of effectively producing decomposition damage predictions similar to the model produced by Chen J. et al.

The six model variations were originally created by Chen J. et al. to show the influences of the applied electric current and applied heat flux on the model for the individual cases of the two current components C and D [69]. Current component C is characterized by low magnitude and long duration while current component D is short and high magnitude. The published results showed that under current component C, the applied heat flux contributed the most to the high temperatures in the fastener and the immediate surrounding CFRP composite laminate. The results showed that under current component D, the applied electric current caused significant Joule heating, which raised temperatures more than the applied heat flux. It was concluded that the main causes of damage under current components C and D are heat flux and electric current, respectively. Furthermore, the development and use of a finite element simulation model to make damage predictions and the comparison of said damage predictions to experimental results, which is shown in Fig. 3.3, demonstrated the effectiveness of FEA in modeling lightning current components C and D in a CFRP composite with fastener [69]. In this work, the successful replication of the finite element simulation model, which is validated by comparison of simulation model results, reinforces the findings of Chen J. et al.

5.2 Study Extensions

The first of the extension work performed herein involved applying a copper layer on top of the CFRP composite laminate in the replication model. Tests were performed using several copper layer thicknesses for current component C and current component D. The maximum temperature results were shown in Fig. 4.5 and Fig. 4.6. It was observed that for both current components, the maximum temperature in the CFRP composite was reduced. However, the introduction and increase in thickness of the copper layer were more effective in reducing the maximum temperature for current component D than current component C. Under current component C, the maximum temperature with the thickest tested copper layer of 0.12 mm was 1760.0°C, which is greater than 300°C. Therefore, decomposition damage would still occur. Under current component D, thicker thicknesses of 0.08 mm, 0.1 mm, and 0.12 mm yielded maximum temperatures less than 300°C, which suggest that no decomposition damage would occur with these thicknesses.

It can be observed that, for both current components, when there is a copper layer present, the maximum temperature appears to decrease following a trend as the thickness of the copper layer increases. The rate of change is greater for current component D as the decrease in maximum temperature is more significant than for current component C. For both current components, it may be possible to create more complete graphs by testing thinner copper layer thicknesses. Using a finer mesh was required to obtain results for current component C with thicknesses of 0.01 mm and 0.005 mm. Using a finer mesh was attempted for similar thicknesses for current component D, but the simulations took too long to converge. It may be possible to achieve convergence for thinner copper layer thicknesses by using an even finer mesh and running the simulations for longer periods of time.

With current component D, it was observed that the maximum temperature did not occur at the end of the simulation interval. It also did not always occur at the same time increment. Therefore, the maximum temperature found may be somewhat dependent on the resolution of the time increments. For example, the "true" maximum may occur at some point between two time increments. Using a smaller time increment for these simulations may allow for more accurate maximum values to be obtained. However, the trend between consecutive thicknesses appears to be consistent, so the influence of the time increment resolution may not be significant.

Along with the evaluation of maximum temperatures, the temperature contour showing the decomposition damage on the top surface of the CFRP composite laminate was displayed for several thicknesses of both current components in Fig. 4.7. With increasing copper layer thickness, the results showed an increase in damage on the surface under current component C and a decrease under current component D. The results may be explained by how the damage under current component C and D is mainly by heat flux and electric current, respectively. It is possible that with the smaller thickness under current component C, more of the heat is transferred downward into the thickness of the fastener and CFRP composite laminate. With the thicker copper layer, more of the heat is transferred outward around the fastener, allowing it to spread over a larger area of the top surface of the laminate. Despite the larger area, the maximum temperature is lower than with thinner copper layers, suggesting that the damage would be less severe. Under current component D, the thicker copper layer presents a larger pathway for the electric current to travel. Since damage under current component D is mostly caused by Joule heating from electric current, the thicker copper layer leads to less Joule heating in the laminate and a smaller damage area.

The second of the extension work performed herein involved using different stacking sequences for the CFRP laminate in the model. The alternative stacking sequences tested were introduced in Table 3.4. The first alternative stacking sequence tested consisted of 45° and -45° layers with 0° layers in-between. The second alternative stacking sequence followed a symmetric pattern with 45°, 0°, -45°, and 90° layers. The tests were performed under current component D in the model that has both applied electric current and heat flux. The results of both tests showed that the decomposition damage extended outward from the fastener in each layer in the direction of the fibers. The results also showed that the direction and length of the decomposition damage can be influenced by the fiber direction of adjacent layers.

The results for the first alternative stacking sequence tested were shown in Fig. 4.8, which displayed the temperature contour of the decomposition damage region for the top four layers superimposed and individually. The superimposed plot showed that the overall pattern of the decomposition damage through the laminate thickness is roughly rectangular in shape. The 0° layer between each of the 45° and -45° layers focuses most of the electric current in the direction of the x-axis, and the decomposition damage can be seen to extend farther along the x-axis than along the y-axis.

The results for the second alternative stacking sequence tested were shown in Fig. 4.9, which included temperature contours, superimposed and individually, for the top four layers as well as individually for the 8th and 9th layers. The superimposed plot showed that the decomposition damage through the laminate is roughly circular in shape. Layers 8 and 9 were included individually in the figure because they demonstrated the longest decomposition damage length in the direction of the y-axis. Layers 8 and 9 are both oriented 90° as the stacking sequence is mirrored between them. The length of decomposition damage in the two layers is likely due to both having the same fiber orientation, which helps to focus the electric current in the y-direction.

The primary differences between the decomposition damage under current component D of the original stacking sequence and the two alternative stacking sequences are the size and shape of the decomposition damage region. The longest length of decomposition damage was 60.2 mm and was observed along the x-axis in the first alternative stacking sequence tested, the results of which are shown in Fig. 4.8. It is about 14.7% greater than the largest damage length observed in the original stacking sequence. Meanwhile, the largest decomposition damage length found in the second alternative stacking sequence was 56.4 mm in the y-direction in the two plies about the stacking sequence symmetry. This extension work helped to display how the decomposition damage may form under current component D with different stacking sequences. It helped show that having adjacent layers in similar or the same direction can lead to longer decomposition damage length.

Chapter 6

Conclusion

The methods of the work herein were described in Chapter 3. The results were presented in Chapter 4 and discussed in Chapter 5. Here, the findings of the work are summarized, and potential future research is described.

6.1 Conclusion

The research involved in this thesis was comprised of replicating the simulated lightning strike on CFRP composite laminate with fastener model by Chen J. et al. and producing comparable decomposition damage results as well as performing further analyses based on the replicated model to explore the effects of either adding a copper outer layer or of using different stacking sequences. The work was successful in replicating the finite element model of Chen J. et al. and in producing similar results. The study reinforces the demonstration of Chen J. et al. that FEA is a tool capable of making reasonable predictions of lightning strike damage on a CFRP composite laminate with a fastener. In addition, the extension work performed provided insight into the effects of adding a copper outer layer as well as using different stacking sequences.

As composite materials continue to be used more in aircraft designs, research has been carried out in recent years to examine the effects of a simulated lightning strike on a CFRP composite laminate. The simulations have been performed experimentally and computationally with finite element analysis. Finite element models have been developed to simulate the effects of a lightning strike on a CFRP composite plate. However, relatively few have investigated the case in which the lightning attaches to a fastener in the composite specimen. Chen J. et al. examined the damage produced by lightning current components C and D in a CFRP composite laminate with a fastener. Their simulations were performed experimentally and computationally with finite element analysis using COMSOL software [69]. Part of the present work involved replicating the finite element simulation model developed by Chen J. et al.

Before replicating the model of Chen J. et al., practice simulations were performed to develop knowledge of the COMSOL finite element software. By using the software to solve various physics-based problems, it was possible to better understand the functionality of the software. Next, the finite element modeling of Chen J. et al. detailed in their publication was examined closely. The model was replicated with several approximations including current waveform and mesh. The replication model was used to produce similar results, and direct comparison of results verified the accuracy of the replication model. The results demonstrated that the damage under current components C and D is mainly caused by heat flux and electric current, respectively.

The extension work that followed the replication of the model of Chen J. et al. involved adding a copper layer to the top of the CFRP composite laminate and, separately, using different laminate stacking sequences. The results of the copper layer addition showed that as the thickness of the copper layer increases, the maximum temperature in the CFRP composite laminate decreases. While damage area results on the top surface of the laminate were varied between current components C and D, the lower maximum temperatures found with thicker copper layers suggest that applying a thicker copper layer will lead to less severe damage overall. In the second part of the extension work, testing the use of different stacking sequences demonstrated that, under current component D, the decomposition damage extends in the direction of the fibers and can have a greater length when adjacent layers have similar or matching fiber orientations. The extension work performed was based on the replication model but has not been verified with experimentation.

6.2 Future Work

The extension work performed revealed several opportunities for future research. As the extension work was purely computational, it would be appropriate to perform experimental tests to verify the accuracy of the new damage predictions. It may be ideal to design the experiments first and then make adjustments to the finite element model based on the conditions of each test. This would allow for test properties and data such as the applied current waveform to be collected and used directly in the finite element study. Being able to compare experimental damage results to numerical results collected for the extension work would allow for the accuracy of the damage predictions to be evaluated and may provide insight into ways the numerical model could be developed further.

In addition to performing experimentation for the extension work completed, there are ways the study can be changed to further explore the lightning strike event. The first of the extension work involved adding a solid copper layer; the traditional LSP method involves adding a copper mesh, which has been modeled in FEA for unnotched laminates [21, 51, 62, 70, 71]. Future work may involve modeling the addition of a copper mesh used in aircraft in place of the solid copper layer. The copper mesh would provide the study with a closer representation of the LSP used in aircraft. Other forms of LSP could also be explored, including novel approaches that utilize carbon nanotubes. In the second part of the extension work, two different stacking sequences were tested. Future work may include testing additional stacking sequences and/or different composite laminates with different material properties. Performing new experimental and numerical studies with different configurations of the simulation of a lightning strike on a CFRP composite laminate will build upon the existing knowledge of the field.

Bibliography

[1] Holm Altenbach, Johannes Altenbach, and Wolfgang Kissing. *Mechanics of Composite Structural Elements*. Springer, 2018.

[2] Qian Zhao, Kai Zhang, Shuang Zhu, Hanyang Xu, Dianguo Cao, Lina Zhao, Ronghua Zhang, and Wuliang Yin. Review on the electrical resistance/conductivity of carbon fiber reinforced polymer. *Applied Sciences*, 9(11):2390, 2019.

[3] Krishan K Chawla. *Composite Materials: Science and Engineering*. Springer, 2019.

[4] Soo-Jin Park. *Carbon Fibers*. Springer, 2018.

[5] Christophe Bouvet. *Mechanics of Aeronautical Composite Materials*. John Wiley & Sons, 2017.

[6] Jihua Gou, Yong Tang, Fei Liang, Zhongfu Zhao, David Firsich, and Jennifer Fielding. Carbon nanofiber paper for lightning strike protection of composite materials. *Composites Part B: Engineering*, 41(2):192–198, 2010.

[7] Paolo Feraboli and Mark Miller. Damage resistance and tolerance of carbon/epoxy composite coupons subjected to simulated lightning strike. *Composites Part A: Applied Science and Manufacturing*, 40(6-7):954–967, 2009.

[8] Martin Gagné and Daniel Therriault. Lightning strike protection of composites. *Progress in Aerospace Sciences*, 64:1–16, 2014.

[9] MA Uman and VA Rakov. The interaction of lightning with airborne vehicles. *Progress in Aerospace Sciences*, 39(1):61–81, 2003.

[10] Society of Automotive Engineers. *Aircraft Lightning Environment and Related Test Waveforms*. SAE ARP5412B, 2013.

[11] FA Fisher, JA Plumer, and RA Perala. Aircraft lightning protection handbook. Technical report, Lightning Technologies Inc. Pittsfield, MA, 1989.

[12] Society of Automotive Engineers. *Aircraft Lightning Zone*. SAE ARP5414B, 2018.

[13] Jinru Sun, Xueling Yao, Xiangyu Tian, Jingliang Chen, and Yi Wu. Damage characteristics of CFRP laminates subjected to multiple lightning current strike. *Applied Composite Materials*, 26(3):745–762, 2019.

[14] Qi Dong, Guoshun Wan, Yunli Guo, Leian Zhang, Xiuting Wei, Xiaosu Yi, and Yuxi Jia. Damage analysis of carbon fiber composites exposed to combined lightning current components D and C. *Composites Science and Technology*, 179:1–9, 2019.

[15] Jinru Sun, Xueling Yao, Wenjun Xu, Jingliang Chen, and Yi Wu. Evaluation method for lightning damage of carbon fiber reinforced polymers subjected to multiple lightning strikes with different combinations of current components. *Journal of Composite Materials*, 54(1):111–125, 2020.

[16] Wayne L Golding. Lightning strikes on commercial aircraft: How the airlines are coping. *Journal of Aviation/Aerospace Education & Research*, 15(1):41–50, 2005.

[17] Paolo Feraboli and Hirohide Kawakami. Damage of carbon/epoxy composite plates subjected to mechanical impact and simulated lightning. *Journal of Aircraft*, 47(3):999–1012, 2010.

[18] Yoshiyasu Hirano, Shingo Katsumata, Yutaka Iwahori, and Akira Todoroki. Artificial lightning testing on graphite/epoxy composite laminate. *Composites Part A: Applied Science and Manufacturing*, 41(10):1461–1470, 2010.

[19] Toshio Ogasawara, Yoshiyasu Hirano, and Akinori Yoshimura. Coupled thermal-electrical analysis for carbon fiber/epoxy composites exposed to simulated lightning current. *Composites Part A: Applied Science and Manufacturing*, 41(8):973–981, 2010.

[20] L Chemartin, P Lalande, B Peyrou, A Chazottes, PQ Elias, C Delalondre, BG Cheron, and F Lago. Direct effects of lightning on aircraft structure: Analysis of the thermal, electrical and mechanical constraints. *Aerospace Lab*, 2012.

[21] G Abdelal and A Murphy. Nonlinear numerical modelling of lightning strike effect on composite panels with temperature dependent material properties. *Composite Structures*, 109:268–278, 2014.

[22] Raúl Muñoz, Sofía Delgado, Carlos González, Bernardo López-Romano, De-Yi Wang, and Javier LLorca. Modeling lightning impact thermo-mechanical damage on composite materials. *Applied Composite Materials*, 21(1):149–164, 2014.

[23] FS Wang, N Ding, ZQ Liu, YY Ji, and ZF Yue. Ablation damage characteristic and residual strength prediction of carbon fiber/epoxy composite suffered from lightning strike. *Composite Structures*, 117:222–233, 2014.

[24] ZQ Liu, ZF Yue, FS Wang, and YY Ji. Combining analysis of coupled electrical-thermal and blow-off impulse effects on composite laminate induced by lightning strike. *Applied Composite Materials*, 22(2):189–207, 2015.

[25] Qi Dong, Yunli Guo, Xiaochen Sun, and Yuxi Jia. Coupled electrical-thermal-pyrolytic analysis of carbon fiber/epoxy composites subjected to lightning strike. *Polymer*, 56:385–394, 2015.

[26] Qi Dong, Yunli Guo, Jingliang Chen, Xueling Yao, Xiaosu Yi, Lu Ping, and Yuxi Jia. Influencing factor analysis based on electrical-thermal-pyrolytic simulation of carbon fiber composites lightning damage. *Composite Structures*, 140:1–10, 2016.

[27] Jin-hua Han, Hui Zhang, Ming-ji Chen, Dong Wang, Qing Liu, Qi-lei Wu, and Zhong Zhang. The combination of carbon nanotube buckypaper and insulating adhesive for lightning strike protection of the carbon fiber/epoxy laminates. *Carbon*, 94:101–113, 2015.

[28] Yichao Li, Renfu Li, Luyi Lu, and Xianrong Huang. Experimental study of damage characteristics of carbon woven fabric/epoxy laminates subjected to lightning strike. *Composites Part A: Applied Science and Manufacturing*, 79:164–175, 2015.

[29] Xiang Ma, Fabrizio Scarpa, Hua-Xin Peng, Giuliano Allegri, Jie Yuan, and Romeo Ciobanu. Design of a hybrid carbon fibre/carbon nanotube composite for enhanced lightning strike resistance. *Aerospace Science and Technology*, 47:367–377, 2015.

[30] Yoshiyasu Hirano, Tomohiro Yokozeki, Yuichi Ishida, Teruya Goto, Tatsuhiro Takahashi, Danna Qian, Shoji Ito, Toshio Ogasawara, and Masaru Ishibashi. Lightning damage suppression in a carbon fiber-reinforced polymer with a polyaniline-based conductive thermoset matrix. *Composites Science and Technology*, 127:1–7, 2016.

[31] Yeqing Wang and Olesya I Zhupanska. Thermal ablation in fiber-reinforced composite laminates subjected to continuing lightning current. In *57th AIAA/ASCE/AHS/ASC Structures, Structural Dynamics, and Materials Conference*, 2016.

[32] Omer Soykasap, Sukru Karakaya, and Mehmet Colakoglu. Simulation of lightning strike damage in carbon nanotube doped CFRP composites. *Journal of Reinforced Plastics and Composites*, 35(6):504–515, 2016.

[33] FS Wang, YY Ji, XS Yu, H Chen, and ZF Yue. Ablation damage assessment of aircraft carbon fiber/epoxy composite and its protection structures suffered from lightning strike. *Composite Structures*, 145:226–241, 2016.

[34] P Naghipour, EJ Pineda, and SM Arnold. Simulation of lightning-induced delamination in un-protected CFRP laminates. *Applied Composite Materials*, 23(4):523–535, 2016.

[35] Li Shulin, Yin Junjie, Yao Xueling, Chang Fei, and Shi Xiaopeng. Damage analysis for carbon fiber/epoxy composite exposed to simulated lightning current. *Journal of Reinforced Plastics and Composites*, 35(15):1201–1213, 2016.

[36] JJ Yin, SL Li, XL Yao, F Chang, LK Li, and XH Zhang. Lightning strike ablation damage characteristic analysis for carbon fiber/epoxy composite laminate with fastener. *Applied Composite Materials*, 23(4):821–837, 2016.

[37] Kunkun Fu, Lin Ye, Li Chang, Chunhui Yang, and Zhong Zhang. Modelling of lightning strike damage to CFRP composites with an advanced protection system. Part I: Thermal-electrical transition. *Composite Structures*, 165:83–90, 2017.

[38] Qi Dong, Guoshun Wan, Yongzheng Xu, Yunli Guo, Tianxiang Du, Xiaosu Yi, and Yuxi Jia. Lightning damage of carbon fiber/epoxy laminates with interlayers modified by nickel-coated multi-walled carbon nanotubes. *Applied Composite Materials*, 24(6):1339–1351, 2017.

[39] JJ Yin, F Chang, SL Li, XL Yao, JR Sun, and Y Xiao. Experimental and numerical simulation analysis of typical carbon woven fabric/epoxy laminates subjected to lightning strike. *Applied Composite Materials*, 24(6):1353–1372, 2017.

[40] Yunli Guo, Qi Dong, Jingliang Chen, Xueling Yao, Xiaosu Yi, and Yuxi Jia. Comparison between temperature and pyrolysis dependent models to evaluate the lightning strike damage of carbon fiber composite laminates. *Composites Part A: Applied Science and Manufacturing*, 97:10–18, 2017.

[41] Gasser F Abdelal and Adrian Murphy. A multiphysics simulation approach for efficient modeling of lightning strike tests on aircraft structures. *IEEE Transactions on Plasma Science*, 45(4):725–735, 2017.

[42] Andrzej Katunin, Katarzyna Krukiewicz, Roman Turczyn, Przemysław Sul, Andrzej Łasica, and Marcin Bilewicz. Synthesis and characterization of the electrically conductive polymeric composite for lightning strike protection of aircraft structures. *Composite Structures*, 159:773–783, 2017.

[43] Andrzej Katunin, Katarzyna Krukiewicz, Roman Turczyn, Przemysław Sul, and Krzysztof Dragan. Lightning strike resistance of an electrically conductive CFRP with a CSA-doped PANI/epoxy matrix. *Composite Structures*, 181:203–213, 2017.

[44] Andrzej Katunin, Przemysław Sul, Andrzej Łasica, Krzysztof Dragan, Katarzyna Krukiewicz, and Roman Turczyn. Damage resistance of CSA-doped PANI/epoxy CFRP composite during passing the artificial lightning through the aircraft rivet. *Engineering Failure Analysis*, 82:116–122, 2017.

[45] FS Wang, XS Yu, SQ Jia, and P Li. Experimental and numerical study on residual strength of aircraft carbon/epoxy composite after lightning strike. *Aerospace Science and Technology*, 75:304–314, 2018.

[46] Ben Wang, Yugang Duan, Zhibo Xin, Xueling Yao, Dilmurat Abliz, and Gerhard Ziegmann. Fabrication of an enriched graphene surface protection of carbon fiber/epoxy composites for lightning strike via a percolating-assisted resin film infusion method. *Composites Science and Technology*, 158:51–60, 2018.

[47] T Kirchdoerfer, A Liebscher, and M Ortiz. CTH shock physics simulation of non-linear material effects within an aerospace CFRP fastener assembly due to direct lightning attachment. *Composite Structures*, 189:357–365, 2018.

[48] Shintaro Kamiyama, Yoshiyasu Hirano, and Toshio Ogasawara. Delamination analysis of CFRP laminates exposed to lightning strike considering cooling process. *Composite Structures*, 196:55–62, 2018.

[49] Hanqing Che, Martin Gagné, PSM Rajesh, Jolanta E Klemberg-Sapieha, Frederic Sirois, Daniel Therriault, and Stephen Yue. Metallization of carbon fiber reinforced polymers for lightning strike protection. *Journal of Materials Engineering and Performance*, 27(10):5205–5211, 2018.

[50] H Chen, FS Wang, XT Ma, and ZF Yue. The coupling mechanism and damage prediction of carbon fiber/epoxy composites exposed to lightning current. *Composite Structures*, 203:436–445, 2018.

[51] Juhyeong Lee, Thomas E Lacy Jr, Charles U Pittman Jr, and Michael S Mazzola. Thermal response of carbon fiber epoxy laminates with metallic and nonmetallic protection layers to simulated lightning currents. *Polymer Composites*, 39(S4):E2149–E2166, 2018.

[52] Juhyeong Lee, Thomas E Lacy Jr, Charles U Pittman Jr, and Michael S Mazzola. Temperature-dependent thermal decomposition of carbon/epoxy laminates subjected to simulated lightning currents. *Polymer Composites*, 39(S4):E2185–E2198, 2018.

[53] Qi Dong, Guoshun Wan, Lu Ping, Yunli Guo, Xiaosu Yi, and Yuxi Jia. Coupled thermal-mechanical damage model of laminated carbon fiber/resin composite subjected to lightning strike. *Composite Structures*, 206:185–193, 2018.

[54] P Foster, G Abdelal, and A Murphy. Understanding how arc attachment behaviour influences the prediction of composite specimen thermal loading during an artificial lightning strike test. *Composite Structures*, 192:671–683, 2018.

[55] P Foster, G Abdelal, and A Murphy. Modelling of mechanical failure due to constrained thermal expansion at the lightning arc attachment point in carbon fibre epoxy composite material. *Engineering Failure Analysis*, 94:364–378, 2018.

[56] P Foster, G Abdelal, and A Murphy. Quantifying the influence of lightning strike pressure loading on composite specimen damage. *Applied Composite Materials*, 26(1):115–137, 2019.

[57] Senqing Jia, Fusheng Wang, Weichao Huang, and Bin Xu. Research on the blow-off impulse effect of a composite reinforced panel subjected to lightning strike. *Applied Sciences*, 9(6):1168, 2019.

[58] Juhyeong Lee, Thomas E Lacy Jr, Charles U Pittman Jr, and Michael S Mazzola. Comparison of lightning protection performance of carbon/epoxy laminates with a non-metallic outer layer. *Journal of Reinforced Plastics and Composites*, 38(7):301–313, 2019.

[59] Juhyeong Lee, Thomas E Lacy Jr, Charles U Pittman Jr, and JN Reddy. Numerical estimations of lightning-induced mechanical damage in carbon/epoxy composites using shock wave overpressure and equivalent air blast overpressure. *Composite Structures*, 224:111039, 2019.

[60] Kunkun Fu and Lin Ye. Modelling of lightning-induced dynamic response and mechanical damage in CFRP composite laminates with protection. *Composite Structures*, 218:162–173, 2019.

[61] Jikui Zhang, Xianglin Zhang, Xiaoquan Cheng, Yanwei Hei, Liying Xing, and Zhibao Li. Lightning strike damage on the composite laminates with carbon nanotube films: Protection effect and damage mechanism. *Composites Part B: Engineering*, 168:342–352, 2019.

[62] FS Wang, Y Zhang, XT Ma, Z Wei, and JF Gao. Lightning ablation suppression of aircraft carbon/epoxy composite laminates by metal mesh. *Journal of Materials Science & Technology*, 35(11):2693–2704, 2019.

[63] SLJ Millen, A Murphy, G Abdelal, and G Catalanotti. Sequential finite element modelling of lightning arc plasma and composite specimen thermal-electric damage. *Computers & Structures*, 222:48–62, 2019.

[64] SLJ Millen, A Murphy, G Catalanotti, and G Abdelal. Coupled thermal-mechanical progressive damage model with strain and heating rate effects for lightning strike damage assessment. *Applied Composite Materials*, 26(5-6):1437–1459, 2019.

[65] SLJ Millen, A Murphy, G Abdelal, and G Catalanotti. Specimen representation on the prediction of artificial test lightning plasma, resulting specimen loading and subsequent composite material damage. *Composite Structures*, 231:111545, 2020.

[66] SLJ Millen and A Murphy. Understanding the influence of test specimen boundary conditions on material failure resulting from artificial lightning strike. *Engineering Failure Analysis*, 114:104577, 2020.

[67] Jinru Sun, Yafeng Li, Xiangyu Tian, Yugang Duan, Xueling Yao, and Ben Wang. Experimental and numerical analysis of damage mechanisms for carbon fiber-reinforced polymer composites subjected to lightning strikes. *Engineering Failure Analysis*, 118:104894, 2020.

[68] Juhyeong Lee, Thomas E Lacy Jr, and Charles U Pittman Jr. Coupled thermal electrical and mechanical lightning damage predictions to carbon/epoxy composites during arc channel shape expansion. *Composite Structures*, 255:112912, 2021.

[69] Jian Chen, Xiaolei Bi, Juan Liu, and Zhengcai Fu. Damage investigation of carbon-fiber-reinforced plastic laminates with fasteners subjected to lightning current components C and D. *Applied Sciences*, 10(6):2147, 2020.

[70] TM Dhanya and CS Yerramalli. Lightning strike effect on carbon fiber reinforced composites – effect of copper mesh protection. *Materials Today Communications*, 16:124–134, 2018.

[71] Ting Hu and Xiongqing Yu. Lightning performance of copper-mesh clad composite panels: Test and simulation. *Coatings*, 9(11):727, 2019.

[72] Robert M Jones. *Mechanics of Composite Materials*. Taylor & Francis, 1999.

[73] Ever J Barbero. *Finite Element Analysis of Composite Materials Using Abaqus*. CRC Press, 2013.

[74] JN Reddy. *An Introduction to Nonlinear Finite Element Analysis: With Applications to Heat Transfer, Fluid Mechanics, and Solid Mechanics*. Oxford University Press, 2015.

[75] Ioannis Koutromanos. *Fundamentals of Finite Element Analysis: Linear Finite Element Analysis*. John Wiley & Sons, 2018.

[76] COMSOL, Inc. *COMSOL Multiphysics, version 5.4*. Burlington, MA, 2018.

[77] COMSOL, Inc. *Documentation for COMSOL, version 5.4*. Burlington, MA, 2018.

[78] The MathWorks, Inc. *MATLAB R2020b*. Natick, MA, 2020.

[79] YA Çengel and AJ Ghajar. *Heat and Mass Transfer: Fundamentals and Applications*. McGraw-Hill Education, 2014.

Christopher L. Trapp

EDUCATION

The Pennsylvania State University *Expected Graduation: May 2021*

Bachelor of Science in Mechanical Engineering with Honors in Mechanical Engineering

Thesis Title: “Multiphysics Finite Element Analysis of Lightning Strike Effects on Carbon Fiber Reinforced Polymer Composites”

- Thesis Supervisor: Dr. Amir Barakati
- Thesis Co-supervisor: Dr. Joseph M. Mahoney

Peer Tutor (During Fall/Spring Semesters) *Fall 2018 – Spring 2021*

RESEARCH & PROJECTS

Senior Capstone Project:

- Designed automated sheet stacking assembly for industry sponsor

HECBC Spring 2020 Poster: “Investigating the Performance of an Aircraft Mechanical Altimeter”

Pfriemer Adaptive Equipment Project (PADEP):

- Worked in multidisciplinary team to design prototype of adjustable wheelchair basket

HONORS & AWARDS

2017 President’s Freshman Award
2018 President Sparks Award
Lehigh Valley General Scholarship *2018 – 2019*
Sproesser Scholarship *2020 – 2021*
Dean’s List *All Completed Fall/Spring Semesters*

WORK EXPERIENCE

Solar Atmospheres Inc. *Souderton, PA*
Maintenance Intern *Summer 2018, 2019, 2020*

Responsibilities:

- Worked with maintenance department staff to support workplace safety and productivity
- Used AutoCAD and Autodesk Inventor to create 2D and 3D models, perform analysis of structural components, and prepare technical drawings
- Examined, edited, and tested PLC and HMI configurations
- Communicated with other companies for manufacturing of design components